

Boundary-Layer Meteorol (2014) 152:245–276
DOI 10.1007/s10546-014-9926-2

ARTICLE

Advances in Air–Sea CO₂ Flux Measurement by Eddy Correlation

Byron W. Blomquist · Barry J. Huebert ·
Christopher W. Fairall · Ludovic Bariteau ·
James B. Edson · Jeffrey E. Hare · Wade R. McGillis

Received: 10 August 2013 / Accepted: 18 March 2014 / Published online: 12 April 2014
© The Author(s) 2014. This article is published with open access at Springerlink.com

Abstract Eddy-correlation measurements of the oceanic CO₂ flux are useful for the development and validation of air–sea gas exchange models and for analysis of the marine carbon cycle. Results from more than a decade of published work and from two recent field programs illustrate the principal interferences from water vapour and motion, demonstrating experimental approaches for improving measurement precision and accuracy. Water vapour cross-sensitivity is the greatest source of error for CO₂ flux measurements using infrared gas analyzers, often leading to a ten-fold bias in the measured CO₂ flux. Much of this error is not related to optical contamination, as previously supposed. While various correction schemes have been demonstrated, the use of an air dryer and closed-path analyzer is the most effective way to eliminate this interference. This approach also obviates density corrections described by Webb et al. (*Q J R Meteorol* 106:85–100, 1980). Signal lag and frequency response are a concern with closed-path systems, but periodic gas pulses at the inlet tip provide for precise determination of lag time and frequency attenuation. Flux attenuation corrections are shown to be <5% for a cavity ring-down analyzer (CRDS) and dryer with a 60-m inlet line. The estimated flux detection limit for the CRDS analyzer and dryer is a factor of ten better than

B. W. Blomquist (✉) · B. J. Huebert
Department of Oceanography, University of Hawaii, Honolulu, HI, USA
e-mail: blomquis@hawaii.edu

C. W. Fairall
Earth System Research Laboratory, NOAA, Boulder, CO, USA

L. Bariteau
Cooperative Institute for Research in Environmental Sciences, University of Colorado, Boulder, CO, USA

J. B. Edson
Department of Marine Sciences, University of Connecticut, Groton, CT, USA

J. E. Hare
Joint Institute for Marine and Atmospheric Research, University of Hawaii, Honolulu, HI, USA

W. R. McGillis
Lamont Doherty Earth Observatory, Columbia University, Palisades, NY, USA

for IRGAs sampling moist air. While ship-motion interference is apparent with all analyzers tested in this study, decorrelation or regression methods are effective in removing most of this bias from IRGA measurements and may also be applicable to the CRDS.

Keywords Air–sea gas exchange · Carbon dioxide · Cavity ring-down spectrometer · Eddy correlation · Flux measurement · Infrared gas analyzer

1 Introduction

Eddy correlation (EC) is a well established surface flux technique in carbon cycle research. Continuous flux observations are now routine across a global network of land-based sites (<http://fluxnet.ornl.gov>, Baldocchi et al. 2001), largely directed at determining net ecosystem exchange over seasonal time scales. The terrestrial research community has a clear focus on flux bias issues that potentially integrate to large errors in net ecosystem exchange, and a general consensus exists concerning standardized methods and data analysis procedures (e.g., Lee et al. 2004).

In contrast, the objectives of marine EC flux measurements are focused on short time scales of 10 min to 1 h, to examine the effects of physical forcing factors (McGillis et al. 2001a; Huebert et al. 2004; Marandino et al. 2007; Miller et al. 2010; Fairall et al. 2011). The principal motivation for air–sea flux measurements is the development and validation of bulk flux and empirical gas transfer models for prognostic analysis of the ocean’s role in energy budgets and biogeochemical cycles. The oceans are a net sink for carbon dioxide—roughly 2 Pg C year^{-1} or one-third of the estimated annual anthropogenic production of CO_2 (Takahashi et al. 2002; Sabine et al. 2004; Jacobson et al. 2007; Takahashi et al. 2009). Global carbon cycle models are well developed, and in these models the air–sea CO_2 transfer coefficient, k_c , is often simulated by polynomial functions of the mean 10-m wind speed (\bar{u}_{10}). A variety of quadratic and cubic wind-speed dependencies have been proposed (Wanninkhof 1992; Wanninkhof and McGillis 1999; Nightingale et al. 2000; McGillis et al. 2001a; Ho et al. 2006; Sweeney et al. 2007; Prytherch et al. 2010; Edson et al. 2011). In a study comparing the effects of quadratic and cubic representations, Takahashi et al. (2002) found a 70 % enhancement in both annual CO_2 uptake and wind-speed sensitivity for the cubic k_c model. An uncertainty this large lends urgency to the task of identifying and quantifying the factors controlling air–sea gas exchange.

Contrasting experimental approaches for air–sea gas transfer studies have been developed: tracer studies utilizing ambient gases (Rn , $^{14}\text{CO}_2$) or deliberately introduced tracers (^3He , SF_6) that integrate the flux over time scales of days to years (Wanninkhof 1992; Nightingale et al. 2000; Ho et al. 2006; Sweeney et al. 2007; Ho et al. 2011), and direct EC flux measurements of CO_2 on hourly time scales (McGillis et al. 2001a, 2004; Kondo and Tsukamoto 2007; Weiss et al. 2007; Miller et al. 2009, 2010; Prytherch et al. 2010; Edson et al. 2011; Lauvset et al. 2011). In general, EC measurements tend to support a cubic wind-speed dependence for k_c while results from tracer studies assume a quadratic model, although one long-term EC study at an inland-sea site with limited fetch also seems consistent with a quadratic model (Weiss et al. 2007). Solubility differences are surely one source of variability in k among the various gases, but a full explanation of the discrepancies remains elusive. There are large uncertainties associated with both experimental approaches. Improving EC measurement precision and accuracy is therefore a high priority.

While the principles of EC flux measurements on land and sea are the same, marine studies present several unique problems. The oceanographic community has yet to reach a consensus

Table 1 Recent ship-based eddy-correlation CO₂ flux studies

Project	Location	CO ₂ analyzer	References
GasEx-98	North Atlantic	LI6262	McGillis et al. (2001a,b)
GasEx-01	Equatorial Pacific	LI6262	McGillis et al. (2004)
Arkona Spar ^a	Baltic	LI7500	Weiss et al. (2007)
MR05-03	Equatorial Indian	LI7500	Kondo and Tsukamoto (2007)
G.O. Sars	North Atlantic	LI7500 ^b	Lauvset et al. (2011)
Polarfront	North Atlantic	LI7500	Prytherch et al. (2010)
Knorr07	North Atlantic	LI7500 ^c	Miller et al. (2009, 2010)
SO GasEx	Southern Ocean	LI7500	Edson et al. (2011)
DYNAMO	Equatorial Indian	LI7500/LI7200 ^d	This report
TORERO	Equatorial Pacific	CRDS ^e	This report

^a Spar buoy, shallow water, limited fetch

^b Shrouded to limit optical contamination

^c LI7500 converted to closed-path, with dryer

^d Two LI7200, with and without dryers

^e Picarro G1301-f, with dryer

on methods to deal with all of these issues. Except in shallow coastal areas where fixed platforms are feasible, measurements must be made from a ship, drifting spar or moored buoy. Motion induced by waves and by changes in ship heading prevent a fixed coordinate frame of reference; high-rate wind measurements must therefore be corrected for platform tilt, rotation and velocity. Inevitable airflow distortion caused by the ship's superstructure should be minimized and mean wind speeds corrected for its effects. Equipment must function in a hostile environment of salt spray and sooty emissions, where opportunities for cleaning and servicing in-situ sensors are often limited by hazardous conditions. Other general issues related to errors in EC flux measurements are well known: sampling uncertainty, signal attenuation in sampling tubes and closed path analyzers, and density effects (Webb et al. 1980; Lee and Massman 2011). Many of these problems can be corrected during data processing or minimized by appropriate experimental design. Perhaps most importantly, air–sea CO₂ fluxes are quite small, often $< 3 \text{ mmol m}^{-2}\text{d}^{-1}$ ($1.5 \times 10^{-3} \text{ mg CO}_2 \text{ m}^2 \text{ s}^{-1}$), yielding a concentration standard deviation of at most a few tenths of a ppm on a background concentration of ≈ 390 ppm. A small flux over the vast expanse of the ocean is nevertheless significant to the global carbon cycle. This places a premium on superior signal-to-noise performance and freedom from interferences.

Marine CO₂ flux measurements have been made for at least 15 years. Several studies reporting ship-based EC measurements of CO₂ flux are listed in Table 1. Flux measurements with closed-path infrared gas analyzers (CP-IRGA) on early cruises (e.g. GasEx-98 and -01) were largely successful, despite numerous measurement challenges. However, early trials revealed an IRGA interference related to platform motion. Water vapour cross-sensitivity, inherent to the broadband infrared method, contributes further uncertainty (Fairall et al. 2000; McGillis et al. 2001a). In general, the flux detection limit using these instruments was unfavourable over much of the ocean surface, where the magnitude in CO₂ partial pressure difference between the atmosphere and ocean ($|\Delta p\text{CO}_2|$) is often < 20 ppm.

Subsequent studies tended to prefer the open-path gas analyzer configuration (OP-IRGA) due to inherent advantages in frequency response, power consumption and wind measure-

ment synchronization. The popular choice has been a commercial instrument commonly used in terrestrial flux studies: the LI7500 (LI-COR Biosciences, Lincoln, Nebraska, USA). Unfortunately, the effects of optical contamination and water vapour cross-sensitivity are potentially severe with this design and complex corrections are required (Kohsiek 2000; Prytherch et al. 2010; Edson et al. 2011). Much of the discrepancy between the observed and expected fluxes reported by Kondo and Tsukamoto (2007) may stem from this interference. As a result, flux measurement accuracy and precision have not improved. A case can be made that early CP-IRGA measurements were superior, although Prytherch et al. (2010) and Edson et al. (2011) demonstrate some success in correcting the OP-IRGA water cross-sensitivity in post-processing. Corrections, however, are an order of magnitude larger than the flux.

Miller et al. (2010) have used an OP-IRGA in a modified closed-path configuration with an air dryer, yielding substantial improvement in flux measurement precision. A smaller, weather-proof version of the CP-IRGA with a very short sample inlet tube has recently become available (LI-COR model LI7200), as have fast, high-sensitivity closed-path trace gas analyzers based on cavity-enhanced infrared absorption and cavity ring-down spectrometry. Clearly, technology is advancing and new instruments are gaining wide acceptance in the carbon cycle research community.

It is appropriate at this time to summarize what has been learned over the last decade of ship-based CO₂ flux studies, examine the latest technical innovations, and begin the discussion towards a set of recommended methods and data analysis procedures for EC flux measurements at sea. Our objectives in this paper are to examine the relative performance of new analyzers with respect to the established methods and discuss the most significant errors in the CO₂ flux measurement, showing how they may be eliminated, minimized or at least identified and removed from the dataset. Flux data from two recent field programs will be used as a basis for critical evaluation of new methods. We conclude with a set of recommendations that seem to offer the best flux measurement precision under typical conditions for ship-based deployments.

To narrow the scope of this review, we will not discuss the error in motion-corrected vertical wind, which is independent of the CO₂ method and often less significant. For the same reason, we do not analyze the error in the computed gas transfer coefficient, k_c , which involves additional uncertainty in the determination of seawater $p\text{CO}_2$.

Finally, a note on terminology and notation: the vertical flux of scalar x by EC is traditionally represented as

$$F_x \equiv \overline{w'x'}, \quad (1)$$

where w is the vertical wind-vector component, a prime denotes deviation from the mean, and the overbar signifies an average over the flux sampling interval, typically 10–30 min. For this discussion, we define CO₂ flux in mole fraction units (ppm m s⁻¹); for mass or mole density units, a density factor would be included in (1). Wind variables u and v denote along-wind and cross-wind components, respectively. In all equations we use c to denote CO₂ mole fraction (moles of CO₂ per mole of air, wet or dry), T for temperature in °C and q for specific humidity, computed as absolute humidity divided by moist air density.

2 Instrumental Methods

Commercial variants of the CP-IRGA have been available for many years (e.g. LI-COR models LI6262, LI7000 and more recently the LI7200 model). All of these measure H₂O simultaneously with CO₂ concentration. Compensation for zero-drift and time response effects in

the infrared detector are necessary, and a band-broadening correction is computed for CO₂ based on the measured H₂O mole fraction (see LI-COR Application Note 129, and note that LI-COR uses the term cross-sensitivity to refer to detector time response effects). Newer versions of the CP-IRGA measure optical cell temperature and pressure, enabling a real-time computation of mole fraction from the measured molar density concentration. Except for the LI7200, CP-IRGAs are bench-scale laboratory instruments and must be located in a protected enclosure. The obvious disadvantages are frequency attenuation in sample line tubing (low-pass filtering) and a time lag between the wind-speed and gas concentration measurements. Both of these problems are mitigated by appropriate experimental design.

An open-path IRGA employs the same operational principles in a weather-proof enclosure suited to installation on sampling towers for in-situ measurements. Several early designs were developed (Jones et al. 1978; Ohtaki and Matsui 1982; Kohsiek 1991; Auble and Meyers 1992) but the LI-COR LI7500 is the OP-IRGA in widespread use at this time. However, with an open-path optical cell it is not possible to measure temperature and pressure in the sample volume with sufficient speed and accuracy for a high-precision computation of mole fraction. Open-path IRGA CO₂ concentrations are typically computed as molar or mass density with appropriate density and dilution corrections applied as necessary.

Motion-related interference is a problem for all IRGAs at sea. This effect may correlate with residual motion contamination in the vertical wind measurement, leading to errors in the computed flux. Water vapour interference is perhaps the most significant problem. In theory, the LI-COR algorithm accounts for water effects but the correction is not perfect. For a situation of a small CO₂ flux in the presence of a large H₂O flux, imprecision inevitably leads to bias in the computed CO₂ concentration. Because the interference correlates with water vapour flux (and vertical wind), the resulting $w'c'$ cospectrum is often dominated by water vapour crosstalk, leading to as much as a factor-of-ten error in the computed CO₂ flux.

Advances in tuneable diode laser technology led to the development of “cavity-enhanced” spectroscopic methods suitable for trace gas flux studies at ppm and ppb levels. Cavity ring-down spectrometers (CRDS) were first developed more than 20 years ago (O’Keefe and Deacon 1988) and analyzers for a variety of gases and analytical applications are commercially available (Picarro Inc., Santa Clara, California, USA). A similar method based on direct absorbance, Off-Axis Integrated Cavity Output Spectroscopy or OA-ICOS, is a more recent development (O’Keefe et al. 1999; Baer et al. 2002). As with the CRDS, OA-ICOS analyzers for a variety of gases are manufactured commercially (Los Gatos Research, Mountain View, California, USA).

With cavity-enhanced methods, pressure broadening of the absorption line leads to cross-sensitivity with other components in the gas mixture. Water vapour is once again the principal offender. A correction for line broadening is therefore necessary, and most analyzers include a water measurement in addition to the specific gases of interest. Because these are bench-scale instruments requiring sample inlet tubing, the usual caveats with respect to time lag and spectral attenuation also apply. In both methods, cavity pressure and temperature are carefully controlled and mole fraction may be computed with high precision.

3 Experimental

Carbon dioxide flux measurements were included in two recent field programs as part of an ongoing effort to develop and evaluate new methods. In this section we present a brief overview of the experimental conditions and cruise details relevant to the flux tests.

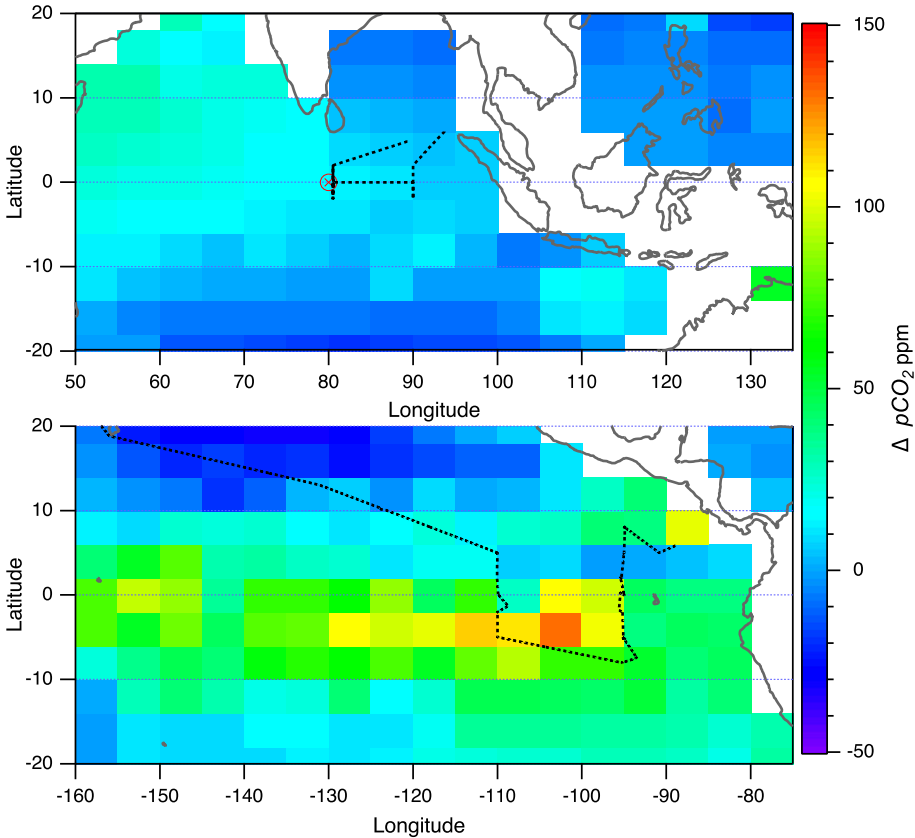


Fig. 1 DYNAMO (Indian Ocean) and TORERO (Pacific Ocean) cruise tracks. $\Delta p\text{CO}_2$ is plotted as the climatological mean for November–December (DYNAMO) and January–February (TORERO), from Takahashi et al. (2009). The DYNAMO study area is a weak source region for CO_2 with $\Delta p\text{CO}_2 \approx +30$ ppm. The TORERO cruise track transitioned from a weak sink area at $10^\circ\text{--}20^\circ\text{N}$ into a very strong source region south of the equator in the east Pacific cold-tongue, where $\Delta p\text{CO}_2 > +100$ ppm

3.1 DYNAMO

Project CINDY2011/DYNAMO (Cooperative Indian Ocean Experiment on Inter-seasonal Variability in Year 2011/Dynamics of the Madden-Julian Oscillation) was a multi-national, multi-platform investigation of ocean-atmosphere interaction in the equatorial Indian Ocean. As one of three platforms providing DYNAMO surface observations, the ship R/V Roger Revelle occupied a station near 0°N , 80°E for the period August 2011–February 2012, with periodic transits to Phuket, Thailand for resupply (see Fig. 1). In this report we focus on Leg 3, from 7 November to 8 December 2011.

The NOAA/ESRL portable flux system (Fairall et al. 1997, 2003) on the R/V Roger Revelle recorded 10 Hz wind and motion measurements, bulk meteorological variables and sea-surface temperature (SST). Four CO_2 IRGAs were installed in the following configurations: two LI7500 OP-IRGAs and one LI7200 CP-IRGA (University of Connecticut), mounted near the wind and motion sensors on the ship's forward mast, and one LI7200 (NOAA/ESRL) installed in a shipping container laboratory on the deck, drawing air from a teflon sampling

tube extending up to the location of the mast flux sensors (30 m, 9.5 mm internal diameter). In this paper we report results from only one LI7500, but the two were comparable in performance. Because the LI7200 cavity pressure sensor has limited differential range, pressure drop considerations restricted the main sample line flow rate to $<40\text{ L min}^{-1}$ STP for the laboratory instrument (Reynolds number, $Re > 5,000$). This analyzer sub-sampled the high-flow inlet at $\approx 4\text{ L min}^{-1}$ STP and a pressure of $\approx 940\text{ hPa}$. A 200-tube Nafion air dryer (PD-200T-24-SS, Perma Pure LLC, Toms River, New Jersey, USA) was used with the laboratory analyzer to reduce sample air dewpoint to $< -15^\circ\text{C}$; water vapour band-broadening and dilution corrections for the laboratory LI7200 analyzer were therefore negligible. Particles $>0.7\ \mu\text{m}$ in diameter were filtered from the laboratory LI7200 sample stream (47 mm Whatman GF/F). The mast mounted LI7200 flow rate was 17 L min^{-1} through a 1 m by 9.5 mm internal diameter inlet tube. Both LI7200 analyzers record high-rate cell temperature and pressure for automated computation of dry CO₂ mole fraction. Optics for the LI7500 OP-IRGA were rinsed daily with distilled water to limit the effects of surface contamination.

A small equilibrator system and LI-COR 840 CO₂/H₂O analyzer from the Lamont-Doherty Earth Observatory were used to measure air–sea $\Delta p\text{CO}_2$ from the ship's clean sea-water supply. Measurements alternated between the atmospheric and equilibrator gas samples. A Nafion air dryer was used on the LI840 sample stream (0.8 L min^{-1}) to obtain dry air concentrations.

Fluxes from the three IRGA analyzers were computed from the standard “dry” mole fraction output of the LI7200 and the raw molar density output of the LI7500, with the latter corrected for dilution, density perturbations and vertical heave hydrostatic effects using a combination of fast and slow temperature and humidity measurements, as in Edson et al. (2011) (see Sects. 6.1, 6.2). Cospectra were computed from linearly detrended, motion-corrected vertical wind velocity and fast CO₂ fluctuations in 10-min segments. Filtering criteria for relative wind direction, ship manoeuvre parameters and reasonable limits on other variables such as motion correction variances were applied to select optimal measurement conditions: specifically, relative wind within $\pm 90^\circ$ of the bow, heading standard deviation $< 5^\circ$ and ship velocity standard deviation $< 1\text{ ms}^{-1}$. In addition, limits on the time rate-of-change in CO₂ mole fraction, along-wind turbulent flux and cross-wind turbulent flux were used to select for steady-state conditions (see discussion in Sect. 6.5).

3.2 TORERO

Project TORERO (Tropical Ocean Troposphere Exchange of Reactive Halogen Species and Oxygenated volatile organic compounds) was a multi-platform field program focussing on the distribution, reactivity and abundance of oxygenated organics and halogen radicals over the eastern Pacific, from Costa Rica south to Chile. Surface observations on the NOAA ship R/V Ka'imimoana were performed from 10°N to 10°S along the 110°W and 95°W TAO buoy lines. The cruise covered the period 25 January–27 February 2012, including transit from Honolulu, Hawaii at the start and to Costa Rica at the conclusion (see Fig. 1).

A flux instrument package of wind and motion measurements equivalent to the DYNAMO system was installed on the R/V Ka'imimoana. Sensors were mounted at the top of a 10-m meteorological tower on the ship's bow. Data acquisition hardware and a CRDS fast CO₂ analyzer (Picarro model G1301-f) were located in the instrumentation laboratory, $\approx 40\text{ m}$ aft of the bow tower. Compared to DYNAMO, sample inlet tubing was longer with more than double the flow: $\approx 60\text{ m}$, 9.5 mm internal diameter, and 80 L min^{-1} STP ($Re > 11,000$). Air pressure was $\approx 700\text{ hPa}$ at the analyzer inlet. Flow into the analyzer was controlled at $\approx 4.5\text{ L min}^{-1}$ STP and, as in DYNAMO, an identical Nafion air dryer removed water vapour

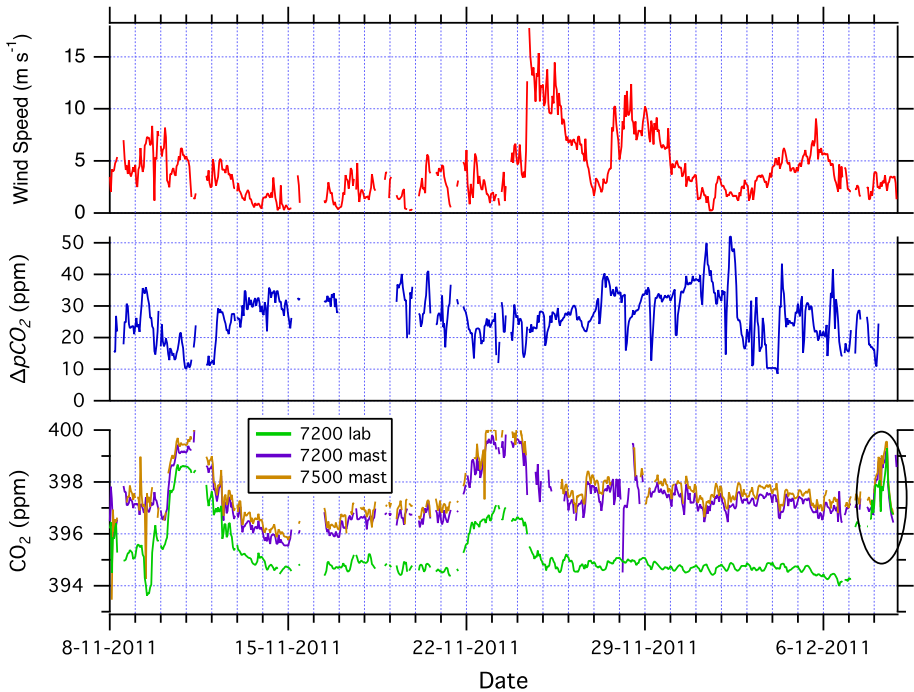


Fig. 2 DYNAMO Leg 3: time series of hourly mean wind speed, $\Delta p\text{CO}_2$ and atmospheric dry CO_2 mole fraction from three IRGA analyzers. An offset of 2–3 ppm is evident between the dry air laboratory LI7200 measurement and mast-mounted analyzers. For the *circled segment* at the end of the leg, the Nafion dryer was removed from the laboratory LI7200 for a direct comparison with moist air measurements. Without the dryer, the laboratory LI7200 “dry” mole fraction output closely tracks the mast “dry” mole fraction measurements (see Sect. 6.2)

from the CO_2 sample stream. The TORERO CRDS differs in one respect from a standard G1301 design with dual H_2O and CO_2 measurements; this spectrometer is configured to omit H_2O , devoting all measurement cycles to CO_2 , yielding somewhat improved signal-to-noise performance (typically $\sigma_c < 0.10$ ppm at 10 Hz), but the analyzer must be used with a dryer.

Wind measurements (10 Hz) were corrected for motion interference using the Edson et al. (1998) method. Flux results were processed in 30-min data segments with 10-min overlap (i.e. four 30-min segments per hour). The linear trend was subtracted from each data segment and a Hamming window applied to limit leakage of low frequency drift. Flux results were filtered with basic wind criteria: relative wind direction within $\pm 60^\circ$ of the bow and standard deviation in relative wind direction $< 10^\circ$ per 30-min segment. Additional stationarity criteria and corrections for CRDS motion interference are discussed in Sects. 6.5 and 6.3 respectively.

4 Results: Flux Observations

4.1 DYNAMO: IRGA Analyzers

During DYNAMO wind conditions were light and variable, punctuated by periodic events when the active phase of the Madden-Julian Oscillation (MJO) was observed, starting on 24 November (Fig. 2, upper panel). The atmospheric CO_2 concentration remained constant at

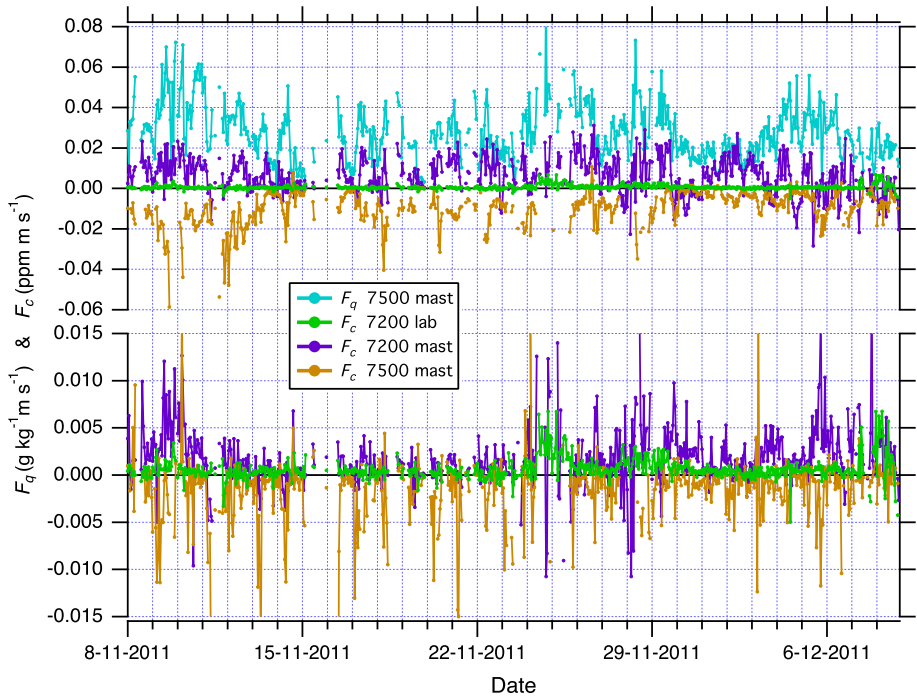


Fig. 3 DYNAMO Leg 3: time series of hourly CO₂ flux ($F_c \equiv \overline{w'c'}$) from the three IRGA instruments. The dry air F_c measurement from the laboratory LI7200 is plotted in *green* as a reference. In the *upper panel*, dry air corrected F_c from mast analyzers (*purple and tan traces*) roughly track specific humidity flux from the mast LI7500 ($F_q \equiv \overline{w'q'}$, *blue trace*) and are about a factor of 14 greater than the laboratory LI7200 reference flux. Note, the mast LI7500 fluxes are negatively correlated to F_q while the mast LI7200 flux correlation is positive. The *lower panel* illustrates application of an additional water vapour cross-correlation correction to the mast analyzers (Edson et al. 2011, Sect. 6.2)

≈ 395 ppm with slight increases on 11 and 23 November (Fig. 2, lower panel). Leg 3 values of $\Delta p\text{CO}_2$ were +20 to +30 ppm, indicative of a weak source region for CO₂ (Fig. 2, middle panel).

Because $\Delta p\text{CO}_2$ for Leg 3 was positive and small, conditions were near the flux detection limit of the IRGA instruments, especially when winds were light (see Sect. 5.2). Throughout Leg 3 we expect a small, positive CO₂ flux. Figure 3 shows that the flux observed by the laboratory LI7200 is near zero or slightly positive, which confirms these expectations. This analyzer shows a clear increase in CO₂ flux during strong winds on 23–24 and 28–29 November. In contrast, results from the mast LI7200 in the upper panel of Fig. 3 show a much larger positive CO₂ flux, correlated to the specific humidity flux (blue trace) and wind speed. The mast LI7500 reports a negative CO₂ flux, often anti-correlated to water vapour flux. Mast flux measurements in Fig. 3 are obtained from dry air corrected mole fractions, and all IRGA CO₂ measurements include the internal LI-COR correction for water vapour cross-sensitivity. Clearly, additional water vapour corrections are necessary for the analyzers sampling moist air. Fluxes corrected with a cross-correlation procedure Edson et al. (2011) are shown in Fig. 3, lower panel, and discussed in Sect. 6.2.

A correlation between CO₂ mole fraction and room temperature was noted for the laboratory-mounted LI7200. Inlet and outlet temperatures fluctuated in synchrony with air

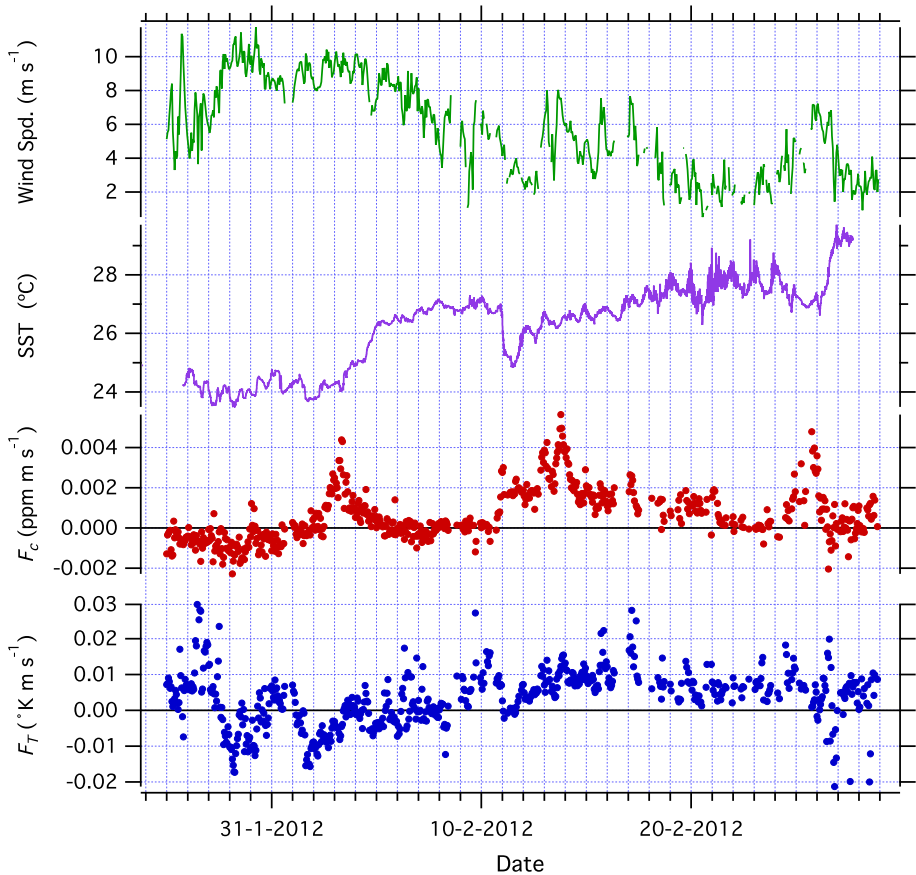


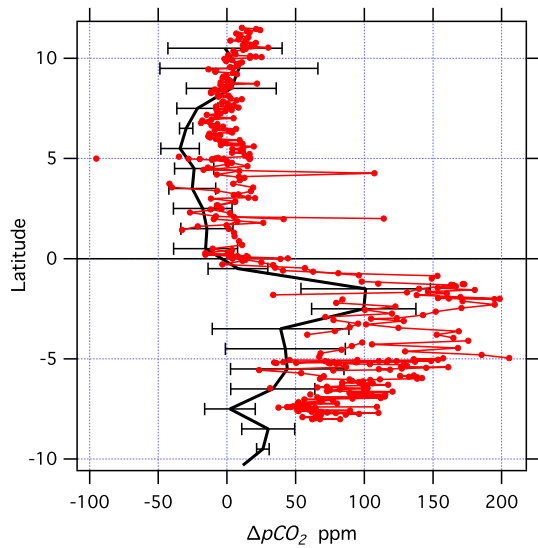
Fig. 4 TORERO: hourly mean wind speed, SST, F_c and sensible heat flux ($F_T \equiv \overline{w'T'}$). The transition to the east Pacific cold tongue on 11 February is evident in the SST and F_c measurements. Prior to 11 February, the transition from a weak CO_2 sink region through a fairly strong, localized source region and then to equilibrium conditions (27 January–10 February) is apparent in the flux results. For the period when flux is near zero (5–10 February) $\sigma_{F_c} = 2.4 \times 10^{-4} \text{ ppm m s}^{-1}$. F_T was generally less than 0.01 K m s^{-1} throughout

conditioner cycling. In theory, the LI-COR algorithm should compensate, but a small residual is apparent in the CO_2 output. Both analyzer and sample line were insulated to damp this artefact. The air conditioner cycling frequency was sufficiently low that concentration drift from room temperature variability should not contribute to flux over 10-min integration times.

4.2 TORERO: CRDS Analyzer

The TORERO cruise track crossed a weak CO_2 sink region south-east of Hawaii, eventually crossing a sharp boundary near the equator into the East Pacific cold-tongue upwelling, a persistent feature in $p\text{CO}_2$ climatology characterized by $\Delta p\text{CO}_2 > +100 \text{ ppm}$ in Fig. 1 (Takahashi et al. 2009). Wind speeds were in excess of 10 m s^{-1} during the transit from Hawaii, but decreased considerably near the equator and into the cold-tongue region.

Fig. 5 TORERO: $\Delta p\text{CO}_2$ in the equatorial region of 95°W and 110°W. *Red trace* estimated from observed F_c and computed k_c . *Black trace* January–February mean $\Delta p\text{CO}_2$ for cruises along 95°W and 110°W from the gridded SOCAT database. *Error bars* are 1σ



CO₂ flux, wind speed and SST are summarized in Fig. 4. Seawater CO₂ measurements were not successful for this cruise due to instrument failure, but on the basis of January–February $\Delta p\text{CO}_2$ climatology in Fig. 1 we expect the initial portion of the transit from Hawaii to be a weak sink region, with $\Delta p\text{CO}_2 \approx -20$ to -30 ppm. The cold tongue region south of the equator should be a strong CO₂ source, and flux observations in Fig. 4 confirm these expectations. The flux detection limit of the CRDS system is more than sufficient to reveal a negative flux across the weak sink region early in the cruise (See Sect. 5.2).

Estimating air–sea disequilibrium from the observed CO₂ flux is an important exercise and provides a check on the quality of flux measurements. In Figure 5 shows, $\Delta p\text{CO}_2$ computed from the CRDS flux data and bulk flux model estimates k_c (COAREG 3.0, Fairall et al. 2011), where $F_c = \alpha k_c \Delta p\text{CO}_2$ and α is the dimensionless solubility. These estimates compare favourably with the January–February mean $\Delta p\text{CO}_2$ from equatorial cruise data in the region from 95°W to 110°W (gridded SOCAT database: <http://www.socat.info>, Sabine et al. 2012). Trends in computed $\Delta p\text{CO}_2$ closely track the multi-year mean latitude gradient for this region.

5 Results: CO₂ Analyzer Performance

5.1 Noise Characteristics

Variance spectra for the CO₂ analyzers are presented in Fig. 6. CRDS background noise is “pink” with a characteristic slope of $\approx -1/2$. There is some indication of turbulent variance following a $-5/3$ power law at low frequencies in the mean TORERO spectrum that may be due to turbulent diffusion of horizontal atmospheric concentration gradients, but signal variance is largely dominated by sensor noise. CRDS noise (1σ) over the flux bandpass of 0.001–5 Hz is 0.07 ppm.

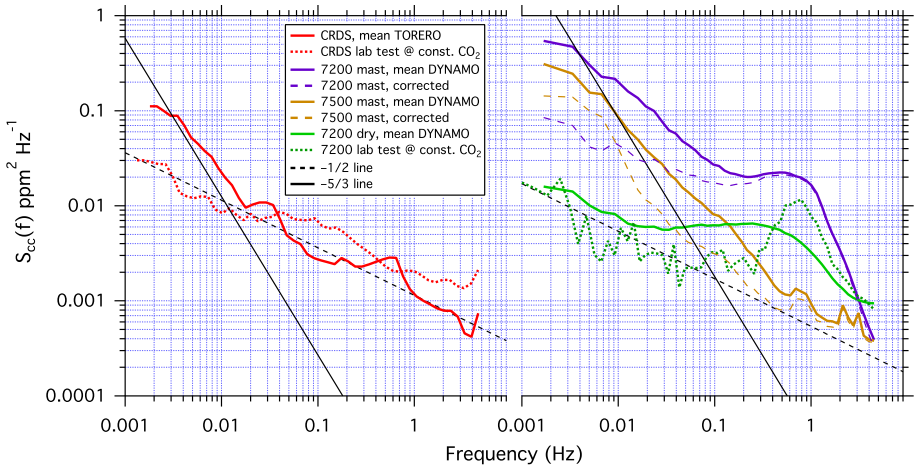


Fig. 6 Mean variance spectra for the CO₂ analyzers. Laboratory tests at constant CO₂ mole fraction are shown as *dotted lines*. *Left panel* CRDS spectra showing a characteristic “pink” noise background with a slope of $\approx -1/2$. The TORERO spectrum shows some indication of a $-5/3$ turbulence relationship at low frequencies, but is otherwise dominated by analyzer noise. *Right panel* IRGA spectra from DYNAMO, which also show a “pink” background noise characteristic. Application of the cross-correlation correction for water vapour interference (Edson et al. 2011, see Sect. 6.2) is shown as *dashed lines*. LI7200 spectra exhibit a broad hump of unknown origin from 0.3 to 0.6 Hz, noted in the raw LI7200 absorbance data for dry air DYNAMO measurements (*green*) and in the dry air laboratory test (*dotted green*), so the feature is not related to water crosstalk or motion

Background noise in the IRGA analyzers may also be “pink” based on the laboratory test spectrum for the LI7200 at constant CO₂ concentration, which is comparable to the CRDS result. However, LI7200 spectra have an unexplained hump at 0.3–0.6 Hz that is unrelated to water vapour or motion interference. This feature is not apparent in cospectra and therefore may not propagate into the flux measurement. A considerable fraction of IRGA CO₂ signal variance in moist air is due to water vapour crosstalk, illustrated by spectra of cross-correlation corrected CO₂ (Fig. 6 dashed lines, see Sect. 6.2).

5.2 Flux Detection Limit

To investigate the flux detection limit, we examine the theoretical flux error as a function of air–sea disequilibrium ($\Delta p\text{CO}_2$) and wind speed (u). The flux error may be specified as a function of variance in both vertical wind (w) and scalar (CO₂) measurements, where CO₂ variance is composed of an atmospheric vertical turbulent flux component ($\sigma_{c_a}^2$) and an “other noise variance” component ($\sigma_{c_n}^2$, arising from analyzer noise, water vapour crosstalk and other interference), and where T_s is the sampling time in sec (see Fairall et al. 2000 and Blomquist et al. 2010),

$$\delta F_c = \frac{2\sigma_w}{\sqrt{T_s}} [\sigma_{c_a}^2 \tau_{wc} + \sigma_{c_n}^2 \tau_{c_n}]^{1/2}. \tag{2}$$

The two terms in (2) are assumed to be independent, with characteristic integral time scales (τ_{wc} and τ_{c_n}). From the scatter in flux measurements under conditions where $|\Delta p\text{CO}_2|$ is very low, and therefore $\sigma_{c_a}^2$ is approximately zero, we can solve (2) for an empirical estimate

of the “other noise” term,

$$\epsilon_n \equiv \sigma_{c_n}^2 \tau_{c_n} \approx \left[\frac{\delta F_c^2 T_s}{4 \sigma_w^2} \right]_{\sigma_{c_a}^2 \approx 0} \tag{3}$$

Quantities σ_w , $\sigma_{c_a}^2$ and τ_{wc} in (2) are stability dependent, and Monin–Obhukov similarity scaling may be used to express the stability dependence of variances through the following relationships,

$$\sigma_w = 1.25 u_* f_w(z/L), \tag{4}$$

$$\sigma_{c_a} = \frac{3 F_c}{u_*} f_c(z/L), \tag{5}$$

where L is the Obukhov length and u_* is the friction velocity. In addition, an empirical relationship (6, below) may be used to specify the integral time scale, where $b = 2.8$ is a constant. The functions f_w , f_{CO_2} and f_τ are similarity relationships specifying stability dependence (Blomquist et al. 2010),

$$\tau_{wc} = b \frac{z}{u_r} f_\tau(z/L), \tag{6}$$

$$f_w(z/L) = (1 + 3 |z/L|)^{1/3}, \quad (z/L < 0) \tag{7a}$$

$$f_w(z/L) = 1 + 0.2 z/L, \quad (z/L > 0) \tag{7b}$$

$$f_c(z/L) = (1 + 20 |z/L|)^{-1/3}, \quad (z/L < 0) \tag{8a}$$

$$f_c(z/L) = 1 + 1.0 (z/L)^{1/2}, \quad (z/L > 0) \tag{8b}$$

$$f_\tau(z/L) = [\min(5, \max(0.5, (1 + 0.6z/L)))]^{-1}. \tag{9}$$

Substitution of (4–9) into (2) yields an expression for the flux error as a function of u and u_* , which can be further extended to the detection limit criterion, $|\Delta pCO_2|(u)$, by assuming an arbitrary error condition (e.g. $\delta F_c/F_c = 1$, or 100% error), integration time $T_s = 3,600$ s, and substitution of the standard bulk flux formulation, $F_c(u) = \alpha k_c(u) \Delta pCO_2$. Ignoring stability, the expression may be simplified somewhat by setting (7–9) to unity,

$$|\Delta pCO_2|(u) = \frac{2.50 u_* f_w}{\alpha k_c \sqrt{3600}} \left[\left(\frac{3 F_c f_c}{u_*} \right)^2 \frac{2.8 z f_\tau}{u_r} + \epsilon_n \right]^{1/2} \tag{10}$$

Here, u_r is the relative wind speed (equivalent to u if the ship is not moving), α is the dimensionless CO₂ solubility and k_c is the gas transfer coefficient. For this exercise, k_c , u_* , α and L were computed from the COAREG 3.0 bulk flux model (Fairall et al. 2011) with air temperature = 19°C, SST = 20°C, wind speeds from 1 to 16 ms⁻¹ and default values for other variables.

Empirical values for the “other noise” term in (3) were determined for periods of near-zero CO₂ flux, yielding the following values (all as ppm² s): $\epsilon_{n,CRDS} = 0.00057$, $\epsilon_{n,7500} = 0.04574$, $\epsilon_{n,7200(dry,lab)} = 0.00867$ and $\epsilon_{n,7200(mast)} = 0.02043$. These values include an additional correction for water vapour interference in the mast-mounted sensors (see Fig. 3, lower panel, and Sect. 6.2). We assume ϵ is a constant, but for analyzers with significant water vapour crosstalk the fraction of noise from that source may in fact have a wind-speed dependence. Note that in (10), F_c is dependent on ΔpCO_2 and u , so an iterative solution is necessary.

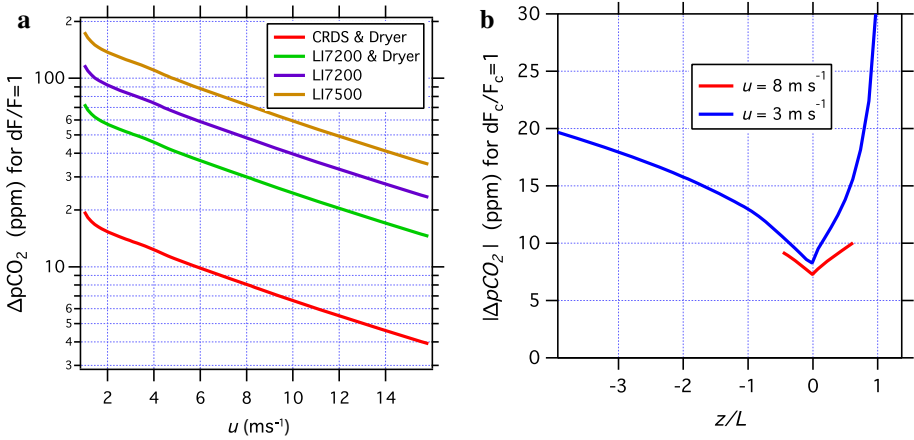


Fig. 7 **a** Flux detection limit criterion versus wind speed for each analyzer, expressed as $|\Delta p\text{CO}_2|$ ppm necessary for $\delta F_c/F_c = 1$ (i.e. 100% error in observed F_c over a 1-h sampling time) under slightly unstable ($z/L = -0.09$, $u = 10 \text{ m s}^{-1}$) and stationary conditions. These results assume a correction for water vapour crosstalk bias in LI7500 and LI7200 analyzers (see Sect. 6.2). $|\Delta p\text{CO}_2|$ computed from (10). **b** Flux detection limit criterion for the CRDS analyzer versus stability parameter z/L at low and moderate wind speeds. z/L and u_* obtained from the COARE 3.0 bulk flux model with all input variables except air temperature held constant: $T_{\text{air}} = 8\text{--}16^\circ\text{C}$, $\text{SST} = 12^\circ\text{C}$, $\text{RH} = 80\%$, and $u = 3$ or 8 m s^{-1} . The flux detection limit increases rapidly for stable conditions and light winds ($z/L > 0.5$, blue trace)

The detection limit criterion $|\Delta p\text{CO}_2|(u)$ computed from (10) for each analyzer is shown in Fig. 7a. The curves represent a theoretical lower limit on $|\Delta p\text{CO}_2|$ for 100% error in the measured flux under slightly unstable ($z/L = -0.09$, $u = 10 \text{ m s}^{-1}$) and stationary conditions. $|\Delta p\text{CO}_2|(u)$ for error conditions other than $\delta F_c/F_c = 1$ scales inversely; for an error of $\delta F_c/F_c = 0.25$, the $|\Delta p\text{CO}_2|$ criterion will be four times greater than indicated in Fig. 7. We also note that, other things being equal, as the SST decreases so does ambient $|\Delta p\text{CO}_2|$ and therefore the flux error will increase with decreasing SST. From Fig. 7 it is clear analyzers with a dryer perform considerably better than those without. This is also generally apparent in the scatter of flux measurements from Figs. 3 and 4. The estimated detection limit for the dry air CRDS measurement represents a factor-of-ten improvement over the earliest measurements with CP-IRGAs.

Figure 7b illustrates the CRDS detection limit as a function of the stability parameter z/L . In this case, k , L and u_* are obtained from COAREG model runs at two wind speeds ($u = 3$ and 8 m s^{-1}) under conditions where all bulk variables other than air temperature are held constant ($T_{\text{air}} = 8\text{--}16^\circ\text{C}$, $\text{SST} = 12^\circ\text{C}$, $\text{RH} = 80\%$ and all other variables at default values). At a moderate wind speed of 8 m s^{-1} , the computed $|\Delta p\text{CO}_2|$ criterion remains acceptable and the stability parameter has a narrow range about zero, even for large air–sea temperature gradients of $\pm 4^\circ\text{C}$ (red trace). In light winds, however, z/L varies over a much wider range (blue trace) and the flux detection limit degrades rapidly under stable conditions when $z/L > 0.5$, or in this case when air temperature exceeds SST by more than 0.5°C .

6 Results: Interferences and Corrections

Instrumental limitations, interference, experimental constraints and meteorological conditions may all contribute to the bias error in EC flux estimates. It is almost always necessary

to apply corrections to computed spectra or covariances to minimize these errors, usually at the expense of a (hopefully small) increase in random error. In this section we discuss the most significant sources of bias error and examine methods to avoid or correct for their effects.

6.1 Density Perturbations

Corrections to molar density fluxes for perturbations caused by heat and pressure fluxes are a well-known issue with EC measurements (Webb et al. 1980; Lee and Massman 2011). For measurements on ships, Miller et al. (2010) have identified an additional pressure/density perturbation resulting from vertical heave. Other dynamic pressure effects are usually minor but may be important at higher wind speeds (Edson et al. 2008; Zhang et al. 2011). The sum of these interferences, if uncorrected, can lead to measurement bias greater than the actual ocean-atmosphere CO₂ flux. The OP-IRGA measurement is most affected by density fluctuations. For most closed-path analyzers, temperature equilibration in sample tubing eliminates the need for a sensible heat-flux correction. Dynamic pressure effects are probably also less significant with the closed-path, but a fast pressure measurement may nevertheless be required for heave-related corrections unless analyzer cell pressure is controlled to a constant value.

Corrections may be applied to computed fluxes using measured latent and sensible heat fluxes, or to the raw CO₂ wet mole fraction time series using simultaneous T , P and water vapour measurements (see Miller et al. 2010). The fundamental assumption of Webb et al. (1980) is a zero surface flux of dry air. The dry air mole fraction of a trace gas is a scalar quantity conserved in vertical motion and is therefore the preferred representation of concentration in conservation equations (Kowalski and Argueso 2011). It is a considerable advantage if the analyzer computes dry air mole fraction in real time from simultaneous measurements of CO₂ and H₂O mole densities, T , and P , eliminating the need for density corrections (Nakai et al. 2011). However, the accuracy of computed dry mole fraction is limited by calibration error and background noise in the T , P and H₂O measurements. Other things being equal, we expect the cavity-enhanced closed-path analyzers, which control the optical cell to constant T and P , will yield better results than an analyzer that relies on fast measurements of T and P for a real-time correction. Where possible, drying the air to a low, constant humidity should be preferable to a computed dilution correction if frequency attenuation effects of the dryer are not severe. In this study, the mean magnitude of density corrections to the DYNAMO LI7500 flux measurements was 35%. For the mast-mounted LI7200 we rely on the analyzer's real-time computation of dry mole fraction, so density corrections are unnecessary.

6.2 Water Vapour Cross-Sensitivity

In addition to density/dilution effects, water vapour presents a direct spectral interference to the CO₂ measurement in IRGA and cavity-enhanced instruments. The combined effects of dilution and spectroscopic interference are illustrated by laboratory test results in Fig. 8. Here, the LI7200 and Picarro CRDS instruments drew air from a common gas sample manifold. Dry air from a compressed gas cylinder had a CO₂ concentration of 423 ppm and negligible water vapour. Upon humidification to a specific humidity of $\approx 11 \text{ g kg}^{-1}$, the observed CRDS CO₂ concentration falls by more than 10 ppm as a result of line broadening and dilution effects. The LI7200 mole fraction, corrected for spectroscopic and detector time response effects in the analyzer but not dilution corrected, fell by 6.5 ppm. Application of the Picarro

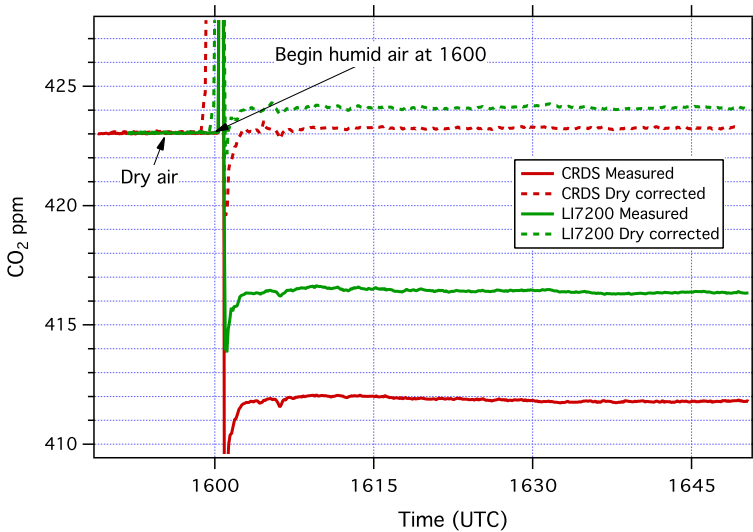


Fig. 8 Laboratory test of $\text{CO}_2\text{-H}_2\text{O}$ cross-sensitivity and dilution corrections. Traces are 10-s averaged data in dry air from a compressed gas cylinder. At 1600 UTC dry air flow was diverted through a Nafion humidifier, increasing dewpoint to $\approx 15^\circ\text{C}$, or $q \approx 11 \text{ g kg}^{-1}$. The observed CRDS concentration, uncorrected for either line broadening or dilution, decreases by more than 10 ppm (*red trace*). The LI7200 wet mole fraction output, corrected for spectral effects in the analyzer but not for dilution, decreases by 6.5 ppm (*green trace*). Application of the Picarro dilution and band-broadening adjustment (Rella 2010) results in a slight over correction of ≈ 0.1 ppm (*red dashed*). The dry mole fraction output of the LI7200 yields a 1.1 ppm overcorrection compared to the true dry air value (*green dashed*)

dilution and band broadening adjustment to the observed CRDS signal (Rella 2010) yields a corrected mole fraction very close to the original dry air value, with a slight overcorrection bias of 0.1–0.2 ppm. The LI7200 dilution corrected “dry” output (dashed green trace) shows an overcorrection bias of 1.1 ppm (0.24 %) that may arise from errors in the LI-COR band broadening correction and/or error in the LI7200 H_2O calibration. In this test, LI7200 humidity compares favourably with that measured using a Vaisala HMP-35 T/RH sensor, so errors in the band broadening and detector time response corrections appear to explain most of the LI7200 bias.

The true CO_2 mole fraction may be represented as the measured value minus a factor proportional to the specific humidity, q , where μ_0 is the proportionality or cross-correlation coefficient for the spectroscopic effects of water vapour at zero frequency,

$$c = c_m - \mu_0 q. \quad (11)$$

Assuming the 1.1 ppm over-correction for the LI7200 instrument in Fig. 8 represents the spectroscopic water vapour crosstalk component in the CO_2 measurement, the coefficient for this case is $\mu_0 = 1.1/11 = 0.10 \text{ ppm kg g}^{-1}$. Towards the end of DYNAMO Leg 3 the Nafion dryer was removed from the laboratory LI7200 for a direct comparison with the mast sensors (highlighted by the circled segment in Fig. 2). Without the dryer, the computed LI7200 “dry” CO_2 mole fraction increases by ≈ 1.7 ppm. The change in q upon removing the dryer is about 17 g kg^{-1} , yielding a second estimate for $\mu_0 = 0.10$, which is identical to the value observed in laboratory tests.

Table 2 DYNAMO: median hourly $F_c (\pm 1\sigma)$ ppm m s⁻¹ for Leg 3

	Median $F_c \pm 1\sigma$ (ppm m s ⁻¹)		
	Base case	PKT ^a	Cross-correlation ^b
LI7200 laboratory ^c	0.00047 ± 0.00049	–	–
LI7200 mast ^d	0.00663 ± 0.00396	0.00061 ± 0.01423	0.00122 ± 0.00155
LI7500 mast ^e	0.00678 ± 0.00314	0.00254 ± 0.00467	0.00081 ± 0.00222

Flux computed as indicated in Sect. 3, de-spiked to remove extreme outliers. Results are shown for the base case (density and dilution corrections applied, where necessary) and two published water vapour crosstalk correction schemes

^a Prytherch et al. (2010)

^b Edson et al. (2011)

^c Dry air data, no density/dilution correction

^d Computed from “dry” mole fraction output, no density/dilution correction

^e Density and dilution correction applied

Equation 11 may be recast in flux terms (Eq. A1, Edson et al. 2011).

$$\overline{w'c'} = \overline{w'c'_m} - \mu_0 \overline{w'q'} \quad (12)$$

From Eq. 12 we therefore expect an error in the observed LI7200 CO₂ flux equal to 10% of the specific humidity flux. Mean DYNAMO latent heat flux of 100W m⁻²s at 29°C and 1,015 hPa equates to a specific humidity flux of ≈ 0.0343 g kg⁻¹ ms⁻¹ and an expected CO₂ flux error of $\approx 3.43 \times 10^{-3}$ ppm m s⁻¹, or about 7.3 times the median dry air LI7200 flux of 4.7×10^{-4} ppm m s⁻¹ (see Table 2). The water vapour crosstalk bias represented by μ_0 is therefore about half of the observed error in the moist air LI7200 CO₂ flux measurements from the mast, which are biased by a factor of 14 in Table 2 (Base case).

Figure 9 is an expanded view of DYNAMO CO₂ measurements for the period when the dryer was removed from the laboratory LI7200. In moist air, the computed dry mole fraction output of the laboratory LI7200 closely tracks the same output from the mast LI7200. In the published algorithm, LI-COR employs a function,

$$\psi(W_f) = 1 + (a_w - 1)W_f, \quad (13)$$

to obtain the corrected equivalent pressure of CO₂, where W_f is the mole fraction of water vapour and a_w is a constant specified as 1.15 for the LI7200 (see Eqs. 4–16, LI-COR LI-7200 Manual, Publication No. 984-10564 and LI-COR Application Note 116). Recomputing CO₂ from raw absorbances using published equations with an adjustment of $a_w = 1.7$ largely removes the offset observed in moist air, at least during this brief period (Fig. 9, black trace). Similar results were obtained by doubling the LI7200 detector time response factor, X_{wc} , in Eqs. 4–16 of the LI7200 manual referenced above. However, recomputing fluxes for the period without the dryer from the corrected time series did not yield a significant improvement in flux variance and bias.

Because both a_w and X_{wc} seem to affect the water vapour correction, the best approach undoubtedly requires a more detailed understanding of the IRGA design and operation. The manufacturer presumably chose optimal values for these factors based on their own testing and calibration procedures, but the true factors may exhibit drift or variance that is difficult to evaluate in the field.

There may be a frequency dependency to the cross-correlation coefficient, such that μ_0 obtained from laboratory tests at constant humidity does not represent the true flux error. In

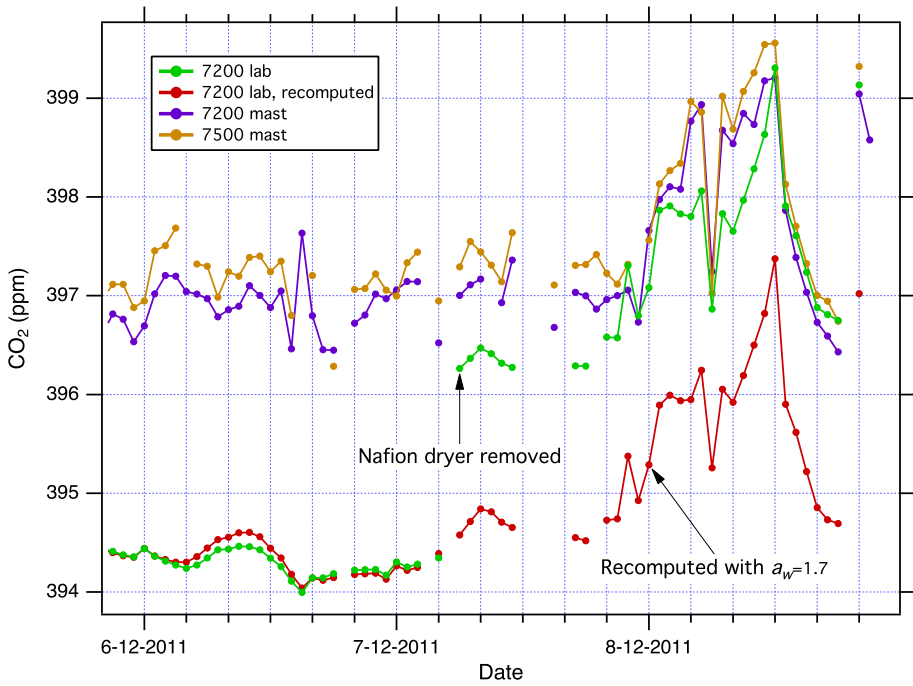


Fig. 9 DYNAMO: CO₂ measurements for 6–8 December. After 0400 UTC on 7 December, the Nafion air dryer was removed from the laboratory LI7200. From that point on, the dry mole fraction output of the laboratory LI7200 closely tracks dry mole fraction from the two mast-mounted IRGAs. Recomputing the laboratory LI7200 dry mole fraction from raw absorbances (red trace) with an adjusted water crosstalk constant ($a_w = 1.7$ rather than 1.15) closely matches the analyzer-computed result for the period with the dryer and does not show a bias following removal of the dryer. Doubling the detector time response factor (X_{wc}) for this IRGA produces a similar effect

this case, the error cross-correlation coefficient may be defined as

$$\mu = \frac{\int \mu(f) C_{wq}(f)}{\int C_{wq}(f)}, \tag{14}$$

where $C_{wq}(f)$ is the $w'q'$ cospectrum and $\mu(f)$ is given by (Edson et al. 2011, Eq. 22) as

$$\mu(f) = \left(1 - \frac{C_{qc}(f)}{C_{qc_m}(f)}\right) \frac{C_{qc_m}(f)}{S_{qq}(f)} \approx \Gamma \frac{C_{qc_m}(f)}{S_{qq}(f)}, \tag{15}$$

where Γ is an estimate for the term in parenthesis. For Γ , the difference from unity is a measure of the true atmospheric $q'c'$ cross-correlation and $\Gamma > 1$ indicates anti-correlation.

Related approaches have been developed to correct water vapour crosstalk and both are applied to the LI7200 and LI7500 mast-measured fluxes in this study. The PKT method (Prytherch et al. 2010) is an iterative correction applied to the raw time series to reduce the observed dependence of CO₂ on relative humidity. The cross-correlation method (Edson et al. 2011) is a spectral approach that seeks to preserve cospectral shape in the corrected result though a determination of $\mu(f)$ in (15). Application of the cross-correlation approach is complicated by the need to account for the true atmospheric component of the $q'c'$ correlation. For SO-GasEx flux measurements, Edson et al. (2011) estimate $\Gamma = 0.88$ from a comparison

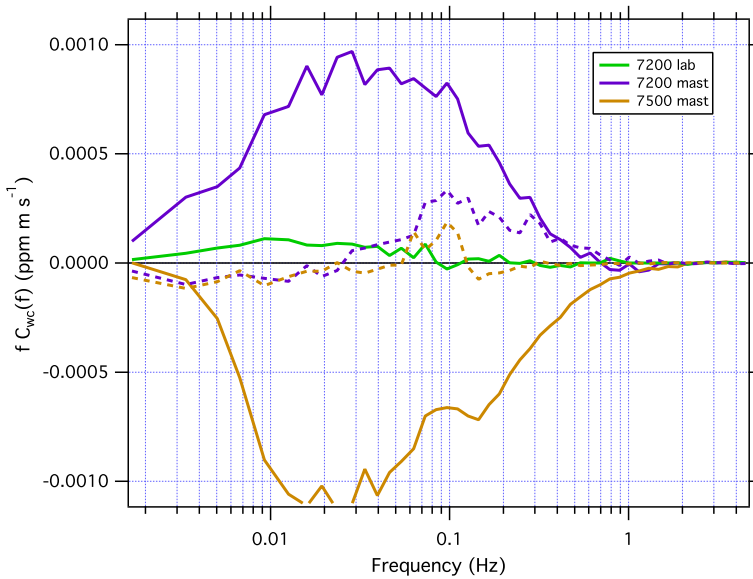


Fig. 10 DYNAMO: project mean cospectra for the IRGAs. Application of the cross-correlation correction for water vapour crosstalk as described in Sect. 6.2 (*dashed lines*) brings the mast IRGA cospectra closer to the dry air LI7200 result. The spectral shape is distorted but fluxes are also very small

with the mean PKT-corrected result, but in general we cannot expect Γ to be a constant. An analysis of water vapour cross-correlation with a third, independent scalar is one approach to obtain Γ , and Appendix A of Edson et al. (2011) illustrates the use of temperature fluctuations for this purpose. This was unsuccessful for DYNAMO, however, due to low sensible heat fluxes. In fact, temperature is not the best scalar for this purpose because $\overline{w'T'}$ approaches zero under near-neutral stability conditions prevalent at sea. An alternate scalar, such as the marine trace gas dimethyl sulphide, might prove more useful but its flux was not measured during DYNAMO. Lacking an independent estimate for the true atmospheric $q'c'$ cross-correlation, mast-measured LI7500 and LI7200 fluxes in this study were scaled to the dry air laboratory LI7200 flux. Best agreement between the moist air and dry air CO₂ flux is obtained with $\Gamma_{7200} = 0.93$ and $\Gamma_{7500} = 1.1$ (project average values), indicating a real atmospheric $q'c'$ cross-correlation that is 7 and 10% of the measured $q'c'$ cross-correlation for these IRGAs during DYNAMO.

Cross-correlation corrected fluxes are plotted on the lower panel of Fig. 3 and summary results for the PKT and cross-correlation approaches (median flux $\pm 1\sigma$) are provided in Table 2. We find the PKT method yields some improvement in flux bias but leads to significantly increased variance in the final result. It is not possible to judge the accuracy of the cross-correlation correction since agreement with the mean dry air flux is the condition used to derive Γ , but the result is hopefully indicative of the improvement in both flux bias and variance that could result when an accurate and independent determination of Γ is available. Figure 10 shows project mean cospectra for the IRGAs and spectral effects of the cross-correlation correction. Water vapour crosstalk is observed at all frequencies across the flux measurement bandpass. Some distortion is apparent in the corrected cospectrum, but fluxes here are very small.

The source of IRGA water vapour crosstalk is often ascribed to hygroscopic contamination of optical surfaces. An analysis of the observed cross-correlation coefficient, $\mu_{\text{obs}} = \overline{q'c'_m}/\sigma_q^2$ (the first term in Eq. A2, Edson et al. (2011), where subscript m refers to the measured or observed value) provides a test of this hypothesis. If optical contamination is a major factor inducing cross-sensitivity, the magnitude of μ_{obs} will decrease significantly following a wash cycle on the LI7500 analyzer. However, during DYNAMO we find no significant shift in μ_{obs} , which varies from -0.2 to -0.4 and remains unaffected when lenses are cleaned with water. Either optical contamination is not the source of additional $q'c'$ cross-correlation or (perhaps less likely) the relevant contaminants are resistant to removal by rinsing. We also observe the laboratory LI7200, a closed-path analyzer sampling filtered air and thus free of optical contamination, nevertheless shows CO₂ flux bias comparable to the mast LI7200 as soon as the dryer is removed (e.g. 8 December in Fig. 3). This further weakens the case for optical contamination as the principal source of a flux bias related to water vapour.

With respect to the use of an air dryer, laboratory tests with both the Picarro CRDS and LI7200 show the uncorrected CO₂ mole fraction remains constant following a large increase in water vapour. The Nafion dryer used in this work holds sample dewpoint to $< -15^\circ\text{C}$ at flow rates up to 5 L min^{-1} STP. At this level, water vapour effects are negligible and the bias noted in Fig. 8 is absent. Use of a dryer was a major focus of the work reported in Miller et al. (2010) and these results confirm the basis of that approach.

6.3 Motion Related Effects for CO₂ Analyzers

Motion interference is an issue unique to ship and aircraft flux measurements and it results from correlation between motion crosstalk errors in both wind-speed and scalar measurements. For IRGAs, the motion effect was noted in the earliest field studies but the exact cause remains uncertain. There may be multiple causes: modulation of the chopper wheel rotation McGillis et al. (2001a), flexing of the source filament Miller et al. (2010), and deformation of the sensor head (Yelland et al. 2009). “Zero calibrations” with closed-path analyzers (McGillis et al. 2001a, 2004) and shrouded “null” open-path sensors (Lauvset et al. 2011; Edson et al. 2011; Prytherch et al. 2010) have both been used as experimental approaches to quantify the ship-motion component of the observed flux. Miller et al. (2010) employ a linear regression between observed CO₂ and the platform angular rates and linear accelerations to remove the motion-induced signal.

For DYNAMO a motion decorrelation, mathematically equivalent to the linear regression approach and analogous to the moisture decorrelation described in Edson et al. (2011), was applied to raw CO₂ and H₂O data prior to subsequent water vapour corrections and flux computations. Motion influence is absent from cospectra in Fig. 10 illustrating the effectiveness of the computed correction to c' , eliminating the correlation with residual motion error in w' .

Motion interference with the CRDS analyzer is apparent in cavity pressure spectra (Fig. 11) and $w'c'$ cospectra (Fig. 12), implying motion sensitivity in the pressure control system that propagates into c' and correlates with residual motion error in w' . The standard CRDS pressure control system uses a single DC solenoid valve. In an attempt to reduce motion sensitivity, Picarro modified the analyzer used in this study by installing two horizontally opposed valves with low-mass actuators. In theory, any motion in one valve will be offset by countervailing motion in the opposed valve. While the modification yields some improvement, TORERO results indicate it is only partially successful. In laboratory experiments, we find CO₂ sensitivity to variable cavity pressure is about $0.112\text{ ppm torr}^{-1}$. However, excess σ_c due to motion (from the integrated area of the motion peak in the CO₂ spectrum) is about

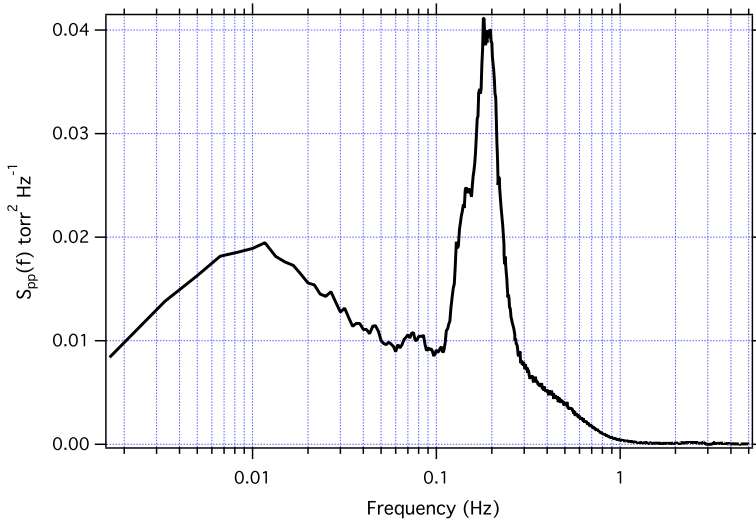


Fig. 11 Mean CRDS cavity pressure spectrum for the first 100 h of the TORERO cruise, when ship motion was greatest. Motion sensitivity of the pressure control system is apparent in the peak at 0.2 Hz

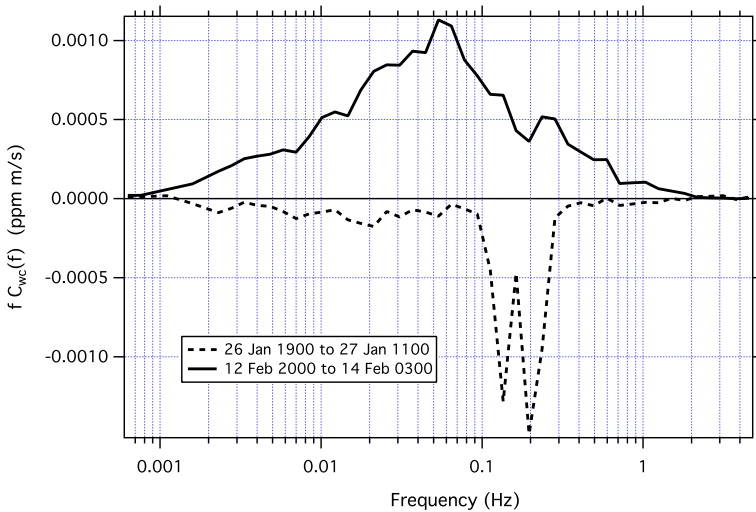


Fig. 12 TORERO: CRDS cospectra for a 16-h period early in the cruise with low negative F_c and high ship motion (*dashed trace*) and a 7-h period of high positive F_c and low ship motion (*solid trace*). The motion effect is evident at 0.1–0.3 Hz in the *dashed trace*. For the few measurements most affected by motion, a corrected estimate of the flux was obtained by fitting a baseline under the cospectral motion peak and removing it from the flux computation

2.5 times greater than that expected for the observed σ_p at a sensitivity of $0.112 \text{ ppm torr}^{-1}$, so additional factors are likely involved.

As with the IRGAs, it should be possible to reduce or eliminate the CRDS motion interference with a regression or decorrelation approach but this was not successful for TORERO, possibly due to installation issues; the motion sensor at the top of the bow meteorological

tower was distant from the CRDS, which was located in a laboratory behind midship and off the centreline. We intend to mount a motion sensor directly on the CRDS analyzer in future field deployments.

For TORERO, motion interference in the CRDS CO₂ measurement was most significant during the outbound transit, when wind speeds were greater and the ship was making maximum headway into the wind and waves. Cospectra from the low-flux, high-motion transit leg and high-flux, low-motion equatorial portion of the cruise are shown in Fig. 12. Motion interference is evident at 0.1–0.3 Hz in the high-motion cospectrum. Flux is computed as the integral of the cospectrum, and for periods where motion interference was significant (707 of 2,677 samples) a corrected flux estimate was obtained by fitting a baseline under the cospectral motion peak and eliminating it from the integral computation. The mean motion induced error for these flux measurements was 28%.

Finally, motion through a scalar concentration gradient near the ocean surface is another possible concern. Does this lead to errors in the computed fluxes? Vertical motion of the analyzer or gas inlet through the CO₂ concentration gradient adds an error to c' , which may not be completely removed by motion corrections to the CO₂ time series, and may correlate with any residual error in w' .

For dimethyl sulphide (DMS) flux measurements, where motion corrections are routinely applied to wind-speed only, Blomquist et al. (2010) show that if the wind-correction error is some fraction, f_{mot} , of the computed motion, and motions are crudely sinusoidal, fractional error from motion through the DMS surface profile is

$$\frac{\Delta F}{F} = \frac{f_{\text{mot}}}{\kappa u_* \bar{z}} \frac{2\sigma_{w_m}^2}{\omega} \overline{\sin(\omega t) \cos(\omega t)}, \tag{16}$$

where $\sigma_{w_m}^2$ is the variance of vertical motion of the sensor, $\kappa = 0.4$ is the von Karman constant, \bar{z} is mean measurement height and $\omega = 2\pi f$ is the angular velocity of the motion. From (16) we conclude motion and concentration terms are in quadrature, or 90° out of phase; the average of the product of sine and cosine is zero, and therefore the fractional error is zero. Thus, from a theoretical perspective, motion through the surface profile should not contribute to the observed flux. A peak at motion frequencies is usually present in the $w'c'$ quadrature spectrum, supporting this conclusion.

However, assumptions of simple fractional dependence and sinusoidal motion are not exactly correct. For extreme high wind-speed and motion conditions ($f_{\text{mot}} = 0.1 \text{ s}^{-1}$, $\bar{u} = 20 \text{ m s}^{-1}$, $u_* = 0.8 \text{ m s}^{-1}$, $\omega = 0.6 \text{ rad s}^{-1}$, $\bar{z} = 18 \text{ m}$, and $\sigma_{w_m}^2 = 6 \text{ m}^2 \text{ s}^2$) the relationship reduces to the following (Blomquist et al. 2010):

$$\frac{\Delta F}{F} = 0.18 \left(2 \overline{\sin(\omega t) \cos(\omega t)} \right). \tag{17}$$

Thus, for the unlikely case that motion and concentration are in phase rather than in quadrature (i.e. $2 \overline{\sin(\omega t) \cos(\omega t)} = 1$) and motion conditions are extreme, the worst case error in DMS flux is $\leq 18\%$. For CO₂, application of a motion correction to the CO₂ mole fraction reduces the potential magnitude of this worst case error considerably.

6.4 Spectral Attenuation

All EC flux measurements are bandwidth limited and may therefore underestimate the true surface flux (see review by Massman and Clement 2004). Resolution of the smallest eddies, at the highest frequencies, is primarily limited by sensor separation and sampling frequency, with additional low-pass filtering effects from the tubing in closed-path systems. Finite flux-

averaging periods and mean removal or detrending methods serve to high-pass filter the lowest frequencies. Over the ocean at moderate wind speeds, under near-stationary and sufficiently turbulent conditions, a 30-min averaging period is sufficient to limit the loss of low frequency flux signal. High frequency losses in closed-path systems are a more significant problem. Two general approaches have been used to deal with spectral attenuation corrections: transfer functions (Moore 1986; Horst 1997; Massman 2000) and spectral similarity methods (Hicks and McMillen 1988).

The flux is often computed as the integral of the observed cospectrum, which can be represented as the integral of the “true” cospectrum times a transfer function, $H(f)$ (e.g. as in Bariteau et al. 2010),

$$F_{xm} = \int_0^{f_n} C_{wxm}(f)df = \int_0^{f_n} C_{wx}(f) [H(f)]^{1/2}df, \quad (18)$$

where the subscript m refers to the measured quantity and f_n is the Nyquist frequency. For a closed-path CO₂ analyzer subject to tube flow spectral attenuation (see Lenschow and Raupach 1991), $H(f)$ may be represented by a simple first-order low-pass filter process characterized by a time constant, τ ,

$$H(f) = [1 + (2\pi f\tau)^2]^{-1}. \quad (19)$$

Note that in (18), we use the square root of $H(f)$ because only the CO₂ signal is attenuated; the w bandwidth is not considered a limiting factor. A model of the “true” cospectrum is required in (18). The normalized flat terrain, neutral-stability scalar cospectrum of Kaimal et al. (1972) is often used,

$$\frac{fC_{wx}(f)}{F_x} = \frac{11n}{(1 + 13.3n)^{1.75}}, \quad n \leq 1.0 \quad (20a)$$

$$\frac{fC_{wx}(f)}{F_x} = \frac{4.4n}{(1 + 3.8n)^{2.4}}, \quad n \geq 1.0 \quad (20b)$$

where the surface normalized frequency $n = fz/\bar{u}_r$ and z is the measurement height.

Given an estimate for τ , Eqs. 19 and 20 may be used to derive an estimate of flux loss from high frequency spectral attenuation

$$R_{\text{attn}}(z, \bar{u}_r) = \frac{\int_0^{f_n} C_{wx}(f, z, \bar{u}_r) [H(f)]^{1/2}df}{\int_0^{f_n} C_{wx}(f, z, \bar{u}_r)df}. \quad (21)$$

A variety of methods can be used to obtain τ : (1) empirical experiments to characterize the transfer function of the inlet and analyzer system (e.g. Blomquist et al. 2010); (2) by invoking spectral similarity, the ratio of the attenuated cospectrum and a reference non-attenuated cospectrum, usually $C_{wT}(f)$, can be used to estimate the cut-off frequency, f_c —the point where the cospectral ratio drops by $1/\sqrt{2}$ from the unattenuated value—and then $\tau = 1/2\pi f_c$; or (3) a step impulse or “puff” in CO₂ concentration can be introduced at the sample inlet tip. The resulting analyzer response can be fit to a low-pass step response function (as in Peters et al. 2001),

$$s(t) = 1, \quad t < t_{\text{lag}} \quad (22a)$$

$$s(t) = \pm \exp\left(\frac{t_{\text{lag}} - t}{\tau_c}\right), \quad t \geq t_{\text{lag}} \quad (22b)$$

where t_{lag} is the flow rate-dependent time delay of the inlet and the sign indicates whether the step is positive or negative.

The alternate approach to attenuation corrections via spectral similarity is useful when a simultaneous high-bandwidth scalar measurement is available for comparison. The sensible heat flux, or $\overline{w'T'}$, as measured by the sonic anemometer, is often used for this purpose. The water vapour flux from an open path sensor (e.g. LI7500) is also suitable, and may be preferable when $\overline{w'T'}$ is near zero. The correction factor is computed by scaling the normalized attenuated $w'c'$ cospectrum to the normalized reference $w'T'$ cospectrum. Usually, a subrange of unattenuated frequencies within the cospectrum is chosen as the basis for the scaling. Computation of the Ogives has also been employed as an expedient for similarity scaling in several recent reports of flux measurements with closed-path sensors (Spirig et al. 2005; Ammann et al. 2006; Miller et al. 2010). In addition to providing a basis for spectral attenuation corrections, the Ogive indicates whether the averaging time is sufficient to capture low frequency flux signal.

The Ogive is defined as the cumulative sum (integral) of the cospectrum (Oncley 1989) from $f = 0$ to f_n and may be computed from a cospectrum averaged into n frequency bins on a logarithmic scale,

$$Og_{wx}(f_m) = \sum_{i=0}^m C_{wx}(f_m) \Delta f_m. \quad (23)$$

for $m = 0, 1, 2, \dots, n$. Normalized to total flux, and plotted together versus log frequency, the Ogive for the attenuated signal lies above the reference Ogive curve. The mean ratio of normalized Ogives, over a range of frequencies where both measurements are assumed to be similar and unattenuated (typically 0.01–0.1 Hz) is an estimate of the flux attenuation factor (see Spirig et al. 2005; Ammann et al. 2006).

For the LI7200 and CRDS closed-path analyzers in this study, a “puff” system was used to synchronize wind and CO₂ measurements, providing a convenient way to determine τ . A burst of nitrogen or compressed air from a solenoid valve, driven by a square-wave trigger with a period of 3–5 s, is injected at the inlet of the main sampling tube, upstream of the dryer, at the beginning of each hour. The time lag between the digital pulse driving the valve and the observed CO₂ response is the signal delay time. A low-pass response function (22) was fit to the rising (valve closure) edge of CO₂ pulses to determine τ . In this case, the second step response in the pulse, when the valve closes, is judged a better representation of an ideal step impulse than the valve opening, which tends to overshoot due to the initial pressure surge.

For TORERO, the mean time constant determined over 705 h of measurements was $\tau = 0.126 \pm 0.008$ s ($f_c = 1.26$ Hz). Values were consistent over the entire project. Attenuation corrections computed from (21) and shown in Fig. 13 represent a 5–6% correction when $\overline{u_r} = 12$ to 14 m s⁻¹ and $\approx 1\%$ when $\overline{u_r} = 3$ – 5 m s⁻¹. For DYNAMO, analysis of the “puff” system response for the LI7200 laboratory analyzer gives $t_{\text{lag}} = 6.2 \pm 0.2$ s and $\tau = 0.38 \pm 0.06$ s, yielding a mean attenuation correction of $\approx 7\%$.

Low sensible heat fluxes during TORERO limited the application of spectral similarity methods. As shown in Fig. 4, $w'T'$ observations were scattered about zero and generally smaller than ± 0.01 K m s⁻¹. This is typical for the tropics, where sensible heat flux is much smaller than latent heat flux. Water vapour flux measurements were not available for TORERO. Figure 14 shows the ratio of normalized cospectra and Ogives for a period when both $\overline{w'T'}$ and $\overline{w'c'}$ yield reasonable cospectra. The Ogives clearly approach the asymptote at both ends, indicating the measurement successfully captured turbulence frequencies contributing to the flux. The normalized Ogive curves are identical within the precision of the

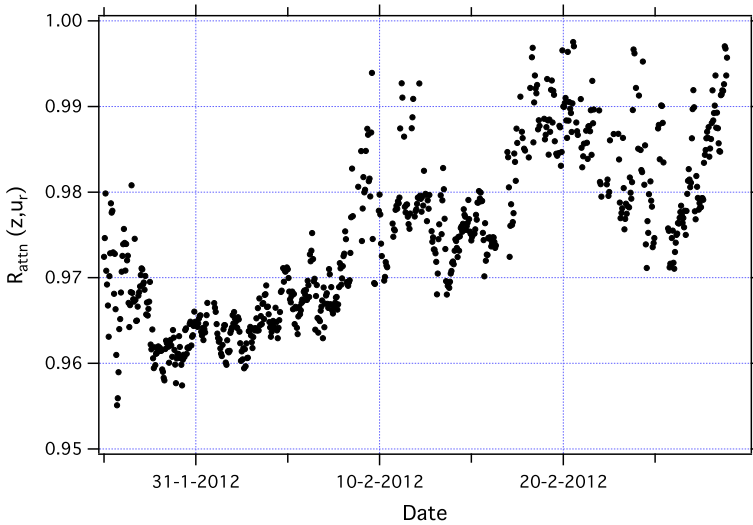


Fig. 13 TORERO: hourly frequency attenuation correction factors computed from the step impulse response to 3-s synchronization “puffs” using (19)–(22). The observed flux is divided by the attenuation correction factor to account for the low-pass filtering effects of the inlet tubing, air dryer and analyzer cavity volume. The correction is less than 4% in almost all cases

data, however, and it is difficult to determine an attenuation factor by scaling the two curves. From the cospectral ratio plot in Fig. 14, it appears f_c should be near 1 Hz, but excessive noise again prevents a precise confirmation of τ by this method. Time constants from “puff” pulses over the same period yield an attenuation correction of $\approx 2.5\%$. In this study, correction factors determined from hourly “puffs” (Fig. 13) are the best measure of signal attenuation.

6.5 Stationarity, Homogeneity and Entrainment

While not an instrumental issue, evaluation of meteorological stationarity is an essential aspect of flux measurements. The use of theoretical cospectral models, such as Kaimal et al. (1972), and invocations of spectral similarity are only valid for steady-state conditions. In general, covariance flux at height z is only equal to the true surface flux under stationary, homogeneous conditions when there is no significant difference between entrainment flux at z_i , the marine boundary-layer inversion height, and z_0 , the surface (Businger 1986). This is especially important in circumstances where surface fluxes are small and the magnitude of surface-flux-driven scalar variance is a minute fraction of the mean background concentration. Edson et al. (2008) provide a nice discussion of flux driven signal variance and mean concentration for DMS and CO₂, gases with greatly differing atmospheric lifetimes. Miller et al. (2010) report a large fraction of air–sea CO₂ flux measurements were discarded on the basis of stationarity criteria, and Blomquist et al. (2012) show a similar sensitivity to stationarity issues in the measurement of air–sea carbon monoxide flux.

The evaluation of steady-state conditions tends to rely on somewhat subjective criteria. One widely used test for stationarity over a 30-min flux averaging interval is based on the fractional difference in covariance flux over 5- and 30-min time scales (Gurjanov et al. 1984; Foken and Wichura 1996; Lee et al. 2004). It is suggested conditions are stationary when the

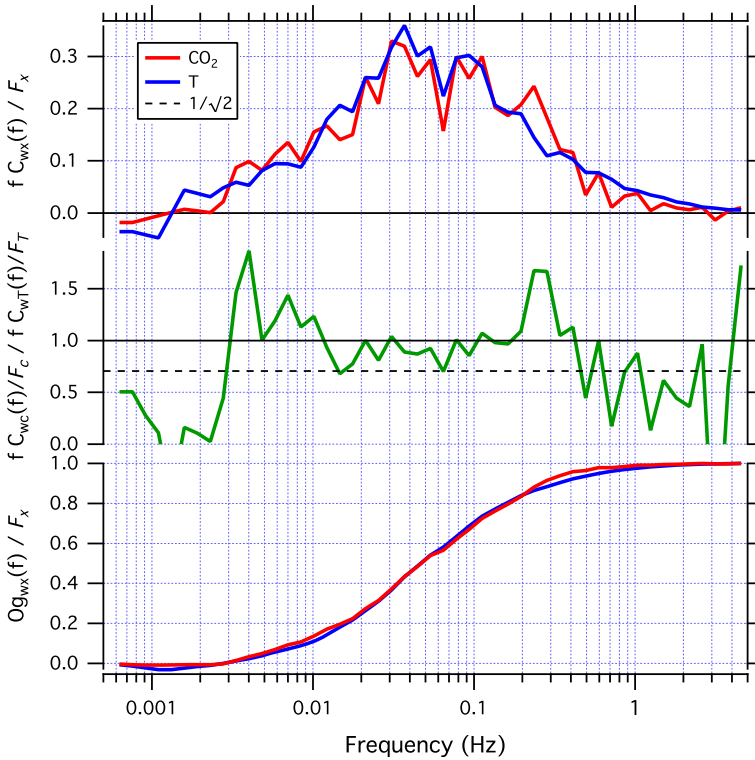


Fig. 14 TORERO: normalized $\overline{w'c'}$ and $\overline{w'T'}$ cospectra, cospectral ratio (*green trace*) and Ogives for 15 February 1600–2300 UTC. This period is characterized by large CO₂ and sensible heat fluxes with moderate winds ($\overline{u}_R = 9.3 \text{ m s}^{-1}$, $\overline{u}_{\text{true}} = 6.2 \text{ m s}^{-1}$). Nevertheless, noise prevents a clear determination of f_c from the cospectral ratio, i.e., the point where the ratio drops by $1/\sqrt{2}$, shown by the *dotted line*. Normalized Ogives for this period are identical within the precision of the data, again preventing precise determination of the small attenuation factor. Ogive curves approach the low frequency asymptote smoothly, indicating 30-min integrations have adequately captured low frequency flux signal

following condition is met:

$$RN_{\text{cov}} = \left| \frac{\overline{(w'x')_5} - \overline{(w'x')_{30}}}{\overline{(w'x')_{30}}} \right| \leq 0.3, \tag{24}$$

where the numerator in (24) is the difference between the 30-min covariance and the mean covariance from 5-min sub-intervals of the same 30-min data segment. In essence, this test asserts that for stationary conditions the flux fraction contributed by frequencies from ≈ 0.001 to 0.007 Hz will be less than 30% of the 30-min covariance flux value. The true proportion of the flux signal expected at these frequencies depends on the specific conditions. To be consistent, wind speed, measurement height and stability could be considered when specifying the length of the sub-interval or the fractional limit. In practice, the test in the form given above is routinely used as a rough filter for non-steady-state conditions.

Among TORERO 30-min flux results passing relative wind and heading criteria ($N = 2,352$) we find 165 observations exceed the 0.30 limit in (24). However, a few obvious outliers manage to pass the test, i.e., measurements where a single 30-min value exceeds

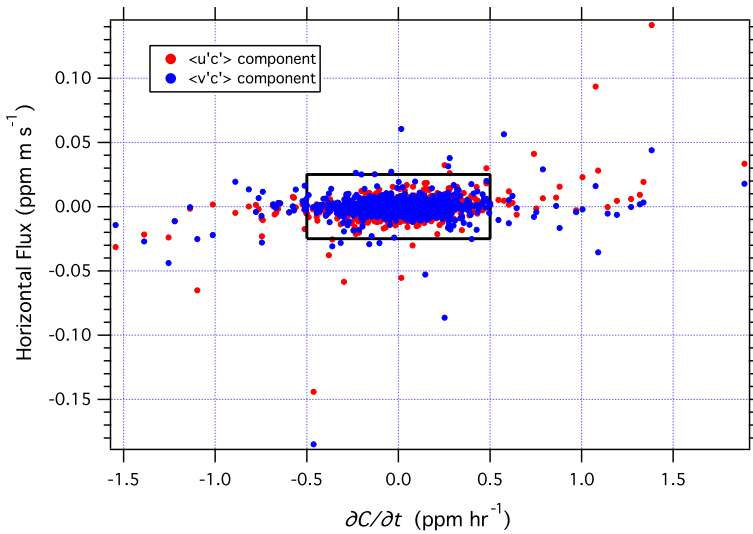


Fig. 15 TORERO CO₂ steady-state criteria: $\overline{v'c'}$ (blue) and $\overline{u'c'}$ (red) turbulent fluxes versus $\partial c/\partial t$ for 30-min data segments. Flux measurements corresponding to points outside the *black bounding box* are excluded from the final hourly mean flux values. Note, limits to the magnitude of horizontal turbulent flux reflected by the bounding box are quite large (10×) compared to the range of vertical turbulent flux in Fig. 4

adjacent values by more than a factor of four; and many values near the flux detection limit are discarded which are not otherwise obviously bad.

Limiting the time rate-of-change in the scalar variable ($\partial c/\partial t$) is another test often used to screen for non-steady-state conditions. Here we extend this test by including horizontal flux components $\overline{u'c'}$ and $\overline{v'c'}$. For DYNAMO and TORERO, the linear trend is removed from each flux data segment and the slope retained as a measure of $\partial c/\partial t$. Figure 15 shows the distribution of horizontal flux components with respect to $\partial c/\partial t$ during TORERO for 2,352 30-min measurements passing relative wind direction criteria. Limits on $\overline{u'c'}$ and $\overline{v'c'}$ of $\pm 0.025 \text{ ppm m s}^{-1}$ and on $\partial c/\partial t$ of $\pm 0.5 \text{ ppm h}^{-1}$ were chosen to exclude extremes (shown as a bounding box in Fig. 15). Admittedly, these limits are also subjective. Applying this test, 72 of 2,352 measurements are rejected, including almost all obvious outliers. Many more observations near the detection limit are retained. For DYNAMO, similar limits were applied, removing 5% of 10-min dry air flux measurements from the laboratory LI7200 that pass other basic criteria.

It should be noted that the subjective limit on the magnitude of horizontal flux in this report ($\pm 0.025 \text{ ppm m s}^{-1}$) is about ten times greater than the range in vertical flux values from Fig. 4. Also, the limit of $\partial c/\partial t < 0.5 \text{ ppm h}^{-1}$ is a very small gradient; at $\bar{u} = 8 \text{ m s}^{-1}$ it represents an along-wind spatial gradient of about 1 ppm per 60 km (0.25% of the mean background CO₂ concentration). This implies that weak spatial gradients in CO₂ can produce a signal variance from horizontal turbulent flux many times larger than CO₂ variance from surface flux alone. A similar situation has been reported for CO flux measurements at sea (Blomquist et al. 2012). Therefore, care should be exercised in choosing the location for field studies; areas affected by even moderate-to-low levels of continental pollution, for example, will provide fewer instances of suitable steady-state conditions, and a large fraction of measurements will be discarded.

Entrainment is an additional source of bias when a significant flux gradient develops between the ocean surface and the marine boundary-layer inversion. For CO₂, this may become a problem when pollution above the boundary layer subsides and is entrained. The situation is difficult to assess from surface measurements alone. Presumably, pollution entrainment leads to increased CO₂ variability, and appropriate stationarity criteria, as discussed above, serve to limit flux bias from this source.

7 Summary and Recommendations

This study provides further confirmation that water vapour interference is the most significant factor limiting the precision and accuracy for ship-based CO₂ flux studies. These results are not definitive with respect to the cause of excessive water vapour crosstalk in the IRGAs, but the interference is apparent in both LI7500 and LI7200 models. Optical contamination is often cited as the principal cause of water vapour interference, but crosstalk is evident in a LI7200 analyzer sampling filtered moist air with no optical contamination (see Figs. 3, 8 and 9). Indeed, the LI7200, when used without a dryer, seems to offer few advantages over the LI7500 for air–sea CO₂ flux measurements. Computed corrections in the LI-COR algorithm appear to be insufficiently precise for measurements of air–sea gas transfer and we cannot recommend CO₂ flux measurements in moist air with the IRGA instruments.

The opposite trend in flux bias between the LI7500 and LI7200 instruments is puzzling and may be related to differences in the internal operation and algorithms of the two IRGAs. The trend in flux bias is consistent for each model: the laboratory LI7200 flux bias is positive and tracks the mast LI7200 flux as soon as the dryer is removed, while fluxes from the LI7500 are biased negatively in this study and in Edson et al. (2011) (see their Fig. 5). Adjustments to the LI-COR a_w and X_{wc} factors may reduce residual water vapour crosstalk in the IRGAs, but DYNAMO results are inconclusive. Optimal values for these factors may vary with time or environmental conditions. Further tests and a more detailed knowledge of the analyzer's internal operation and algorithm are required.

There may be conditions where space and power requirements of a closed-path analyzer, large sampling pump and air dryer will present difficulties—on buoys, near-shore towers or for long-term unattended operation, for example. In this case there appears to be little recourse to the IRGA. But complex corrections will be required (e.g. Prytherch et al. 2010), measurement precision will be poor and a significant fraction of the observations may be discarded. Application of the Edson et al. (2011) cross-correlation correction scheme is facilitated by the measurement of a scalar flux other than temperature that is free of water vapour interference, such as dimethyl sulphide, for an independent determination of the real component of the $q'c'$ correlation, Γ , in (15).

At high flow rates, long sample lines do not significantly degrade CO₂ flux measurements with closed-path analyzers. Cavity-enhanced analyzers operate at low pressure and tolerate considerable pressure drop in the sample line, permitting high flow rates. A large 200-tube Nafion dryer and 80 m by 9.5 mm inlet at 80 L min⁻¹ STP attenuates the flux by <5%. A variety of useful methods exists to determine frequency attenuation and lag time. Hourly gas pulses at the sample inlet have proven most useful in our work, albeit at the expense of greater measurement system complexity. However, it seems worthwhile to verify attenuation corrections with spectral similarity methods when possible. Because the sensible heat flux is often quite small, it is appropriate to deploy the OP-IRGA for water vapour flux, if not for CO₂.

The CRDS instrument shows the greatest promise for significantly improved CO₂ flux measurements from ships. With a dryer, the flux detection limit is an order of magnitude better than IRGAs sampling moist air. We were not able to test real-time water vapour corrections for the CRDS due to the lack of an H₂O channel in our instrument. However, it is clear the dryer does not significantly compromise frequency response and there is much to be gained by eliminating water vapour cross-sensitivity and density correction issues altogether, whichever analyzer is used. Use of an air dryer is highly encouraged.

The issue of motion interference remains a concern for all CO₂ analyzers studied to date. While adjustments to cospectral shape can correct motion artefacts, the application of motion decorrelation or regression methods to the raw CO₂ time series is a fundamentally superior approach. These corrections have been demonstrated for IRGAs (Miller et al. 2010; Edson et al. 2011) and may also be applicable to the CRDS. In the future, analyzer design modifications may reduce or eliminate this problem.

We have not tested an OA-ICOS instrument for CO₂ instruments. However, CO flux measurements at sea have been reported for this instrument under conditions of low to moderate ship motion, without significant interference (Blomquist et al. 2012). Future work should focus on a comparison of the CRDS and OA-ICOS instruments.

Finally, we recommend a careful evaluation of scalar stationarity for flux measurements of CO₂ and other trace gases with long atmospheric lifetimes. Traditional stationarity tests are not always effective near the flux detection limit. An examination of horizontal turbulent fluxes can help improve selectivity of the stationarity test.

Acknowledgments The authors gratefully acknowledge support from NSF grant AGS-1036062, the Office of Naval Research under Grant N00014-10-1-0546 and the NOAA Climate Program Office, Climate Observation Division. We are also grateful for the support and assistance of the officers and crew of the R/V Roger Revelle and R/V Ka'imimoana.

Open Access This article is distributed under the terms of the Creative Commons Attribution License which permits any use, distribution, and reproduction in any medium, provided the original author(s) and the source are credited.

References

- Ammann C, Brunner A, Spirig C, Neftel A (2006) Technical note: water vapor concentration and flux measurements with PTR-MS. *Atmos Chem Phys* 6:4643–4651
- Auble DL, Meyers TP (1992) An open path, fast response infrared absorption gas analyzer for H₂O and CO₂. *Boundary-Layer Meteorol* 59:243–256
- Baer DS, Paul JB, Gupta M, O'Keefe A (2002) Sensitive absorption measurements in the near-infrared region using off-axis integrated-cavity-output spectroscopy. *Appl Phys B*. doi:10.1007/s00340-002-0971-z
- Baldocchi D, Falge E, Gu L, Olsen R, Hollinger D, Running S, Anthoni P, Bernhofer C, Davis K, Evans R, Fuentes J, Goldstein A, Katul G, Law B, Lee X, Malhi Y, Meyers T, Munger W, Oechel W, Paw UKT, Pilegaard K, Schmid HP, Valentini R, Verma S, Vesala T, Wilson K, Wofsy S (2001) FLUXNET: a new tool to study the temporal and spatial variability of ecosystem-scale carbon dioxide, water vapor, and energy flux densities. *Bull Am Meteorol Soc* 82(11):2415–2434
- Bariteau L, Helmig D, Fairall CW, Hare JE, Hueber J, Lang EK (2010) Determination of oceanic ozone deposition by ship-borne eddy covariance measurements. *Atmos Meas Tech* 3:441–455
- Blomquist BW, Huebert BJ, Fairall CW, Faloona IC (2010) Determining the air–sea flux of dimethylsulfide by eddy correlation using mass spectroscopy. *Atmos Meas Tech* 3:1–20
- Blomquist BW, Fairall CW, Huebert BJ, Wilson ST (2012) Direct measurement of the oceanic carbon monoxide flux by eddy correlation. *Atmos Meas Tech* 5:3069–3075
- Businger JA (1986) Evaluation of the accuracy with which dry deposition can be measured with current micrometeorological techniques. *J Clim Appl Meteorol* 25:1100–1124

- Edson JB, Hinton AA, Prada KE, Hare JE, Fairall CW (1998) Direct covariance flux estimates from mobile platforms at sea. *J Atmos Ocean Technol* 15:547–562
- Edson JB, DeGrandpre MD, Frew N, McGillis WR (2008) Investigations of air–sea gas exchange in the CoOP coastal air–sea chemical flux program. *Oceanography* 21(4):34–45
- Edson JB, Fairall CW, Bariteau L, Zappa CJ, Cifuentes-Lorenzen A, McGillis WR, Pezoa S, Hare JE, Helmig D (2011) Direct covariance measurement of CO₂ gas transfer velocity during the 2008 Southern Ocean Gas Exchange Experiment: Wind speed dependency. *J Geophys Res* 116:C00F10
- Fairall CW, White AB, Edson JB, Hare JE (1997) Integrated shipboard measurements of the marine boundary layer. *J Atmos Ocean Technol* 14:338–359
- Fairall CW, Hare JE, Edson JE, McGillis W (2000) Parameterization and micrometeorological measurement of air–sea gas transfer. *Boundary-Layer Meteorol* 96:63–105
- Fairall CW, Bradley EF, Hare JE, Grachev AA, Edson JB (2003) Bulk parameterization of air–sea fluxes: updates and verification for the COARE algorithm. *J Clim* 16:571–591
- Fairall CW, Yang M, Bariteau L, Edson JB, Helmig D, McGillis WR, Pezoa S, Hare JE, Huebert B, Blomquist B (2011) Implementation of the coupled-ocean–atmosphere response experiment algorithm with CO₂, dimethyl sulfide, and O₃. *J Geophys Res* 116:C00F09
- Foken T, Wichura B (1996) Tools for quality assessment of surface-based flux measurements. *Agric For Meteorol* 78:83–105
- Gurjanov AE, Zubkovskij SL, Fedorov MM (1984) Automated multichannel signal processing system based on computer. *Geod Geophys* 26:17–20 (in Russian)
- Hicks BB, McMillen RT (1988) On measurement of dry deposition using imperfect sensors and in non-ideal terrain. *Boundary-Layer Meteorol* 42:79–84
- Ho DT, Law CS, Simth MJ, Schlosser P, Harvey M, Hill P (2006) Measurements of air–sea gas exchange at high wind speeds in the Southern Ocean: implications for global parameterizations. *Geophys Res Lett* 33:L16611
- Ho DT, Wanninkhof R, Schlosser P, Ullman DS, Hebert D, Sullivan KF (2011) Toward a universal relationship between wind speed and gas exchange: gas transfer velocities measured with ³He/SF₆ during the Southern Ocean Gas Exchange Experiment. *J Geophys Res* 116:C00F04
- Horst TW (1997) A simple formula for attenuation of eddy fluxes measured with first-order-response scalar sensors. *Boundary-Layer Meteorol* 82:219–233
- Huebert BJ, Blomquist BW, Hare JE, Fairall CW, Johnson JE, Bates TS (2004) Measurement of the sea–air DMS flux and transfer velocity using eddy correlation. *Geophys Res Lett* 31:L23113
- Jacobson AR, Fletcher SEM, Gruber N, Sarmiento JL, Gloor M (2007) A joint atmosphere–ocean inversion for surface fluxes of carbon dioxide: 1. Methods and global-scale fluxes. *Glob Biogeochem Cycles* 21:GB1019
- Jones EP, Ward TV, Zwick HH (1978) A fast response atmospheric CO₂ sensor for eddy correlation measurements. *Atmos Environ* 12:845–851
- Kaimal JC, Wyngaard JC, Izumi Y, Cote OR (1972) Spectral characteristics of surface-layer turbulence. *Q J R Meteorol* 98:563–589
- Kohsiek W (1991) Infrared H₂O/CO₂ sensor with fiber optics. In: Proceedings of the seventh symposium on meteorological observations and instrumentation. American Meteorological Society, 14–18 January, New Orleans, LA, pp 352–355
- Kohsiek W (2000) Water vapor cross-sensitivity of open path H₂O/CO₂ sensors. *J Atmos Ocean Technol* 17:299–311
- Kondo F, Tsukamoto O (2007) Air–sea flux by eddy covariance technique in the Equatorial Indian Ocean. *J Oceanogr* 63:449–456
- Kowalski AS, Argueso D (2011) Scalar arguments of the mathematical functions defining molecular and turbulent transport of heat and mass in compressible fluids. *Tellus* 63B:1059–1066
- Lauvset SK, McGillis WR, Bariteau L, Fairall CW, Johannessen T, Olsen A, Zappa CJ (2011) Direct measurements of CO₂ flux in the Greenland Sea. *Geophys Res Lett* 38:L12603
- Lee X, Massman WJ (2011) A perspective on thirty years of the Webb, Pearman, and Leuning density corrections. *Boundary-Layer Meteorol* 139:37–59
- Lee X, Massman W, Law B (eds) (2004) Handbook of micrometeorology: a guide for surface flux measurement and analysis. Kluwer, Dordrecht
- Lenschow DH, Raupach MR (1991) The attenuation of fluctuations in scalar concentrations through sampling tubes. *J Geophys Res* 96(D8):15,259–15,268
- Marandino CA, De Bruyn WJ, Miller SD, Saltzman ES (2007) Eddy correlation measurements of the air/sea flux of dimethylsulfide over the North Pacific Ocean. *J Geophys Res* 112:D03301
- Massman WJ (2000) A simple method for estimating frequency response corrections for eddy covariance systems. *Agric For Meteorol* 104:185–198

- Massman WJ, Clement R (2004) Uncertainty in eddy covariance flux estimates resulting from spectral attenuation. In: Lee X, Massman WJ, Law B (eds) Handbook of micrometeorology: a guide for surface flux measurement and analysis. Kluwer, Dordrecht, pp 67–99
- McGillis WR, Edson JB, Hare JE, Fairall CW (2001a) Direct covariance air-sea CO₂ fluxes. *J Geophys Res* 106:16,729–16,745
- McGillis WR, Edson JB, Ware JD, Dacey JWH, Hare JE, Fairall CW, Wanninkhof R (2001b) Carbon dioxide flux techniques performed during GasEx-98. *Mar Chem* 75:267–280
- McGillis WR, Edson JB, Zappa CJ, Ware JD, McKenna SP, Terray EA, Hare JE, Fairall CW, Drennan W, Donelan M, DeGrandpre MD, Wanninkhof R, Feely RA (2004) Air-sea CO₂ exchange in the equatorial Pacific. *J Geophys Res* 109:C08S02
- Miller S, Marandino C, de Bruyn W, Saltzman ES (2009) Air-sea exchange of CO₂ and DMS in the North Atlantic by eddy covariance. *Geophys Res Lett* 36:L15816
- Miller SD, Marandino C, Saltzman ES (2010) Ship-based measurement of air-sea CO₂ exchange by eddy covariance. *J Geophys Res* 115:D02304
- Moore CJ (1986) Frequency response corrections for eddy correlation systems. *Boundary-Layer Meteorol* 37(1–2):17–35
- Nakai T, Iwata H, Harazono Y (2011) Importance of mixing ratio for a long-term CO₂ flux measurement with a closed-path system. *Tellus* 63B:302–308
- Nightingale PD, Malin G, Law CS, Watson AJ, Liss PS, Liddicoat MI, Boutin J, Upstill-Goddard RC (2000) In situ evaluation of air–sea gas exchange parameterizations using novel conservative and volatile tracers. *Glob Biogeochem Cycles* 14:373–387
- Ohtaki E, Matsui T (1982) Infrared device for simultaneous measurement of fluctuations of atmospheric carbon dioxide and water vapor. *Boundary-Layer Meteorol* 24:109–119
- O’Keefe A, Deacon DAG (1988) Cavity ring-down optical spectrometer for absorption measurements using pulsed laser sources. *Rev Sci Instr* 59(12):2544–2551
- O’Keefe A, Scherer JJ, Paul JB (1999) CW integrated cavity output spectroscopy. *Chem Phys Lett* 307:343–349
- Onclay SP (1989) Parameterization techniques in the atmospheric surface layer. PhD Thesis, University of California, Irvine
- Peters G, Fischer B, Munster H (2001) Eddy covariance measurements with closed-path optical humidity sensors: a feasible concept? *J Atmos Ocean Technol* 18:503–514
- Prytherch J, Yelland MJ, Pascal RW, Moat BI, Skjelvan I, Neill CC (2010a) Direct measurements of the CO₂ flux over the ocean: development of a novel method. *Geophys Res Lett* 37:L03607
- Prytherch J, Yelland MJ, Pascal RW, Moat BI, Skjelvan I, Srokosz VA (2010b) Open ocean gas transfer velocity derived from long-term direct measurements of the CO₂ flux. *Geophys Res Lett* 37:L23607
- Rella C (2010) Accurate greenhouse gas measurements in humid gas streams using the Picarro G1301 carbon dioxide/methane/water vapor gas analyzer. White paper, Picarro Inc, Sunnyvale, CA, USA
- Sabine CL, Feely RA, Gruber N, Key RM, Lee K, Bullister JL, Wanninkhof R, Wong CS, Wallace DWR, Tilbrook B, Millero FJ, Peng T-H, Kozyr A, Ono T, Rios AF (2004) The oceanic sink for anthropogenic CO₂. *Science* 305(5682):367–371
- Sabine CL, Hankin S, Koyuk H, Bakker DCE, Pfeil B, Olsen A, Metz N, Kozyr A, Fassbender A, Manke A, Malczyk J, Akl J, Alin SR, Bellerby RGJ, Borges A, Boutin J, Brown PJ, Cai W-J, Chavez FP, Chen A, Cosca C, Feely RA, González-Dávila M, Goyet C, Hardman-Mountford N, Heinze C, Hoppema M, Hunt CW, Hydes D, Ishii M, Johannessen T, Key RM, Körtzinger A, Landschützer P, Lauvset SK, Lefèvre N, Lenton A, Lourantou A, Merlivat L, Midorikawa T, Mintrop L, Miyazaki C, Murata A, Nakadate A, Nakano Y, Nakaoka S, Nojiri Y, Omar AM, Padin XA, Park G-H, Paterson K, Perez FF, Pierrot D, Poisson A, Ríos AF, Salisbury J, Santana-Casiano JM, Sarma VVSS, Schlitzer R, Schneider B, Schuster U, Sieger R, Skjelvan I, Steinhoff T, Suzuki T, Takahashi T, Tedesco K, Telszewski M, Thomas H, Tilbrook B, Vandemark D, Veness T, Watson AJ, Weiss R, Wong CS, Yoshikawa-Inoue H (2012) Surface Ocean CO₂ Atlas (SOCAT) gridded data products. *Earth Syst Sci Data Discuss* 5:781–804
- Spirig C, Neftel A, Ammann C, Dommen J, Grabmer W, Thielmann A, Schaub A, Beauchamp J, Wisthaler A, Hansel A (2005) Eddy covariance flux measurements of biogenic VOCs during ECHO 2003 using proton transfer reaction mass spectrometry. *Atmos Chem Phys* 5:465–481
- Sweeney C, Gloor E, Jacobson AR, Key RM, McKinley G, Sarmiento JL, Wanninkhof R (2007) Constraining global air–sea gas exchange for CO₂ with recent bomb ¹⁴C measurements. *Glob Biogeochem Cycles* 21:GB2015
- Takahashi T, Sutherland SC, Sweeney C, Poisson A, Metz N, Tilbrook B, Bates N, Wanninkhof R, Feely RA, Sabine C, Olafsson J, Nojiri Y (2002) Global sea–air CO₂ flux based on climatological surface ocean pCO₂, and seasonal biological and temperature effects. *Deep Sea Res II* 49:1601–1622
- Takahashi T, Sutherland SC, Wanninkhof R, Sweeney C, Feely RA, Chipman DW, Hales B, Friederich G, Chavez F, Sabine C, Watson A, Bakker DCE, Schuster U, Metz N, Yoshikawa-Inoue H, Ishii M, Midorikawa

- T, Nojiri Y, Kortzinger A, Steinhoff T, Hoppema M, Olafsson J, Arnarson TS, Tilbrook B, Johannessen T, Olsen A, Bellerby R, Wong CS, Delille B, Bates NR, de Baar HJW (2009) Climatological mean and decadal change in surface ocean $p\text{CO}_2$, and net sea-air CO_2 flux over the global oceans. *Deep Sea Res II* 56:554–577
- Wanninkhof R (1992) Relationship between wind speed and gas exchange over the ocean. *J Geophys Res* 97(C5):7373–7382
- Wanninkhof R, McGillis WR (1999) A cubic relationship between air-sea CO_2 exchange and wind speed. *Geophys Res Lett* 26(13):1889–1892
- Webb EK, Pearman GI, Leuning R (1980) Correction of flux measurements for density effects due to heat and water vapour transfer. *Q J R Meteorol* 106:85–100
- Weiss A, Kuss J, Peters G, Schneider B (2007) Evaluating transfer velocity–wind speed relationship using long-term series of direct eddy correlation CO_2 flux measurements. *J Mar Syst* 66:130–139
- Yelland MJ, Pascal RW, Taylor PK, Moat BI (2009) AutoFlux: an autonomous system for the direct measurement of the air–sea fluxes of CO_2 , heat and momentum. *J Oper Oceanogr* 2:15–23
- Zhang J, Lee X, Song G, Han S (2011) Pressure correction to the long-term measurement of carbon dioxide flux. *Agric For Meteorol* 151:70–77